Fluid Chemistry Evolution in Deep-Sea Hydrothermal Environments: Unraveling Mineral-Fluid-Microorganism Interactions through Continuous Culture Experiment

Lise Artigue, Valérie Chavagnac, Christine Destrigneville, David François, Françoise Lesongeur, Anne Godfroy

Deep–Sea Research I 218 (2025) 104456

Contents lists available at ScienceDirect

Deep-Sea Research Part I

journal homepage: www.elsevier.com/locate/dsri

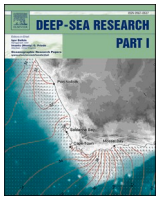

Fluid chemistry evolution in deep-sea hydrothermal environments: Unraveling mineral-fluid-microorganism interactions through continuous culture experiment

Lise Artigue [a,*], Valérie Chavagnac [a], Christine Destrigneville [a], David François [b], Françoise Lesongeur [b], Anne Godfroy [b]

[a] Géosciences Environnement Toulouse, GET, CNRS UMR 5563, UPS, IRD, Université de Toulouse, Toulouse, France
[b] Laboratoire de Biologie et d'Écologie des Écosystèmes marins Profonds, Ifremer, Univ Brest, CNRS, UMR 6197, Plouzané, France

ARTICLE INFO

Keywords:
Gaz-lift bioreactor
Lithium isotopes
Strontium isotopes
Microbial diversity
Geochemical modeling
Lucky strike hydrothermal field

ABSTRACT

This study investigates minerals and microorganisms effects on fluid chemistry through a continuous enrichment culture in a gas-lift bioreactor during the MoMARsat'19 cruise. A sulfate-based chimney and buoyant hydrothermal fluid, both collected *in situ* at the Aisics vent of the Lucky Strike hydrothermal field, were incubated for 18 days under physico-chemical conditions simulating those of diffuse hydrothermal vents. We present the evolution of elemental and Sr, and Li isotopic compositions of the bioreactor fluid, alongside Bacteria and Archaea diversity, and analyze the mineral saturation state of the fluid through geochemical modeling. Our results show that the microbial diversity in the bioreactor reflects that of the sulfate-based chimney. During the initial 168 h, minerals precipitation/dissolution primarily controlled the elemental and Sr isotopic composition of the fluid. From 168 h to 264 h, sulfate-reducing Archaea (Archaeoglobi) disappeared in favor of sulfur-reducing Archaea (Thermoprotei and Thermococci). This shift coincides with a drastic increase in trace element concentrations and less radiogenic $^{87}Sr/^{86}Sr$ ratios, suggesting a possible microbial influence on the fluid. From 264 h onwards, with stable sulfur-reducing archaeal diversity, mineral saturation state primarily controls the elemental composition of the fluid. However, the observed increase in the $^{87}Sr/^{86}Sr$ ratio and $\delta^{7}Li$ correlates with changes in bacterial diversity, notably an increase in Deinococci abundance. This study reveals that in a bioreactor simulating diffuse vent environments related to the sulfur cycle: (i) both microorganism and mineral influence fluid chemistry over time, (ii) shift in microbial diversity appear to affect trace metal concentrations and isotopic signatures, and (iii) the $^{87}Sr/^{86}Sr$ ratio serves as a tracer for mineral-fluid interactions and may be a tracer for microorganism-fluid interactions.

1. Introduction

Hydrothermal vents are distributed along the 67 000 km long mid-ocean ridge system and have a global impact on ocean chemistry, particularly on trace elements and their isotopes (Elderfield and Schultz, 1996; German et al., 2016). These environments, characterized by chemical and physical gradients, offer habitats that support microorganisms growth, making them among the most biologically active regions in the deep ocean (Holden et al., 2012; Zeng et al., 2021). This biological activity involves interactions not only between organisms and chemical species but also between organisms and minerals (Breier et al., 2010; Edwards et al., 2005; Holden et al., 2012; Rogers et al., 2003). Despite significant progress in understanding hydrothermal biogeochemical processes, further research is crucial, particularly in unraveling the complexities of mineral-fluid-microorganism interactions and their influence on biogeochemical cycles (Holden et al., 2012).

To better comprehend water-rock interaction processes, lithium (Li) and strontium (Sr) concentrations and isotopes are widely used to trace geochemical processes notably in geothermal and hydrothermal systems (Araoka et al., 2016; Barker et al., 2008; Chavagnac et al., 2018a; Millot et al., 2010; Wang et al., 2023). However, their complex oceanic budget remains unresolved (Davis et al., 2003; Teagle et al., 2003; Tomascak et al., 2016; Vance et al., 2009). Strontium isotopic ratio ($^{87}Sr/^{86}Sr$ ratio) largely vary across Sr sources or end-members, with high-temperature hydrothermal fluids exhibiting low radiogenic ratio

* Corresponding author.
E-mail address: artigue.get@gmail.com (L. Artigue).

https://doi.org/10.1016/j.dsr.2025.104456
Received 30 August 2024; Received in revised form 16 January 2025; Accepted 24 January 2025
Available online 2 February 2025

Abbreviations:

LSHF Lucky Strike Hydrothermal Field
Buoyant HF Buoyant Hydrothermal Fluid

(0.704230 ± 0.00004, Chavagnac et al., 2018b; Leleu, 2017) compare to seawater (0.709172 ± 0.000012, El Meknassi et al., 2018; El Meknassi et al., 2020). Such variations allow Sr isotopes to trace end-member sources and provide insights into inorganic processes, including mineral dissolution-precipitation and adsorption-desorption, which influence the isotopic $^{87}Sr/^{86}Sr$ ratio of fluids (Huang et al., 2022; McNutt, 2000). Although accumulation of Sr associated to specific Sr isotopic signatures have been observed in various calcifying organisms, including cyanobacteria (Fruchter et al., 2016; Mehta et al., 2023; Stevenson et al., 2014), the potential influence of biotic processes on Sr isotopic fractionation is poorly understood (Mehta et al., 2023). Sr is believed to follow the same cellular pathways as Ca (Mehta et al., 2023; Müller et al., 2018), yet no studies to our knowledge have investigated potential Sr fractionation and the $^{87}Sr/^{86}Sr$ signatures of archaeal and bacterial species. Unlike the $^{87}Sr/^{86}Sr$ ratio, Li isotopes (δ^7Li) provide insights into fractionation processes. Li in seawater is isotopically heavier ($\delta^7Li = +29.5$ ‰) compared to hydrothermal fluids ($\delta^7Li \simeq +3$–6 ‰), due to fractionation processes related to adsorption onto clays and secondary mineral formation (Artigue et al., 2022; Tomascak et al., 2016). δ^7Li can also fractionate through inorganic processes, such as mineral dissolution-precipitation, adsorption-desorption, and ion exchange (e.g., Hindshaw et al., 2019; Li and Liu, 2022; Pistiner and Henderson, 2003; Vigier et al., 2008). In biological systems, Li plays a physiological and biochemical roles (Jakobsson et al., 2017), and fractionation occurs via membrane transport, as specific channels and ion exchanges favor the lighter ^6Li isotope (Poet et al., 2023). Despite their bioaccumulation in marine organisms (Chowdhury and Blust, 2011; Thibon et al., 2021), few studies investigate the Sr and Li elements in relation to aquatic ecosystems (Burger and Lichtscheidl, 2019; Thibon et al., 2021, 2023). It is essential to study the impact of Li and Sr on marine biota, especially considering the growing economic interest on these elements, which leads to studies on their extraction from seawater (Hong et al., 2018; Ryu et al., 2020; Vikström et al., 2013), particularly Li from black smokers hydrothermal vents, which contain 10–20 times more Li than seawater (Chavagnac et al., 2018a; European Commission, 2020). This study combines for the first time the elemental and Li and Sr isotopic tracers of the fluid with thermodynamical modeling (PHREEQC), and microbial diversity analysis, providing new insights into mineral-fluid-microorganism interactions.

Microbial diversity in hydrothermal systems is typically studied using two approaches: *in situ* deep-sea devices (Alain et al., 2004; McCliment et al., 2006; Reysenbach et al., 2000; Rommevaux et al., 2019), or laboratory-based continuous enrichment cultures. The second approach, used in this study, is the only one enabling long-term follow-up of microorganism interactions with dissolved chemical compounds and minerals overtime under controlled conditions. Continuous enrichment cultures in gas-lift bioreactors have proven to be particularly effective for studying deep-sea microorganisms as they maintain steady-state conditions mimicking as closed as possible natural environmental variables (Callac et al., 2015; Godfroy et al., 2000, 2006; Postec et al., 2005a; Postec et al., 2007; Raven et al., 1992). These systems offer significant advantages over batch cultures, including the ability to produce more biomass, support greater microbial diversity, and better simulate hydrothermal environmental conditions. For example, Raven et al. (1992) developed continuous culture techniques for the growth of *Pyrococcus furiosus*, optimizing gas flow rates and dilution rate in the absence of sulfur. Godfroy et al. (2000) explored *Pyrococcus abyssi* growth in both the presence and absence of sulfur, highlighting sulfur's key role in its metabolism. Godfroy et al. (2006) synthesized best practices for optimizing the growth of hyperthermophilic microorganisms for physiological and nutritional studies. Postec et al. (2005b, 2007) used gas-lift bioreactors to cultivate archaeal and bacterial communities from hydrothermal chimney samples. They demonstrated that continuous enrichment cultures better support microbial diversity and metabolic interactions, such as the production of CO_2 and H_2, which sustain autotrophic populations. Lastly, Callac et al. (2015), the sole study using both *in situ* collected inoculum and hydrothermal vent fluids, proposed that interactions between minerals and fluid chemistry create micro-environmental niches that drive microbial diversity which influences sulfur and iron cycling.

Building upon these studies, we used a gas-lift bioreactor to conduct continuous enrichment culture experiments during the MoMARsat'19 cruise. Here, the inoculum, the top youngest part of the Aisics chimneys mainly composed of anhydrite, was collected at the Aisics chimney at the foot step of the Tour Eiffel vent in the Lucky Strike Hydrothermal Field. Anhydrite is commonly found in black smokers and impact marine biogeochemical cycle of calcium and sulfate. The culture medium is the Aisics' buoyant hydrothermal fluid, collected *in situ* between 100 and 150 °C. By collecting both the inoculum and culture medium directly from the Aisics chimney, we provided conditions closer to those found in hydrothermal plumes and diffuse venting, following the approach of Callac et al. (2015). The bioreactor was maintained at near-neutral pH, anaerobic conditions, and high temperatures which are optimal for hyperthermophilic microorganisms as established by earlier studies (Callac et al., 2015; Godfroy et al., 2000, 2006; Postec et al., 2005a; Postec et al., 2007; Raven et al., 1992). While previous studies have focused on sulfur and iron cycling, our study investigates for the first time how mineral-fluid-microorganism interactions affect Sr and Li isotopic signatures. To do so, we followed the chemical evolution of the fluid once in contact with the sulfate-based chimney over an 18-day period, analyzing major and trace elements concentration, as well as Li and Sr isotopes, alongside mineralogy and microbial diversity. Additionally, we discuss the potential impact of microorganisms on the Sr and Li concentrations and isotopic signatures of the fluid medium, unveiling new perspectives on the Li and Sr oceanic biogeochemical cycles.

2. Materials and methods

2.1. Study area

The Lucky Strike Hydrothermal Field (LSHF) is located on the Mid-Atlantic Ridge at 37°17′N and 32°20′W, approximately 400 km to the Southwest of the Azores archipelago (Langmuir et al., 1997; Von Damm et al., 1998). This 1 km^2 hydrothermal vent field lies on a basaltic substratum and comprises 20 to 30 active vents distributed around a fossil lava lake (apart from Capelinhos vent) surrounded by three ancient volcanic cones (Charlou et al., 2000; Escartin et al., 2015; Fouquet et al., 1995; Langmuir et al., 1997; Ondréas et al., 2009; Von Damm et al., 1998). Fig. 1 presents the LSHF bathymetric map, at depths ranging between ~1550 and 1750 m below sea level (mbsl), with 12 active hydrothermal sites. Of specific relevance for this study is the Aisics chimney, located southeast of the fossil lava lake, at the base of the Tour Eiffel hydrothermal edifice.

2.2. Sample collection and onboard processing

During the MoMARsat'19 EMSO-Azores maintenance cruise aboard the *R.V. Pourquoi Pas?* (June–July 2019, Sarradin and Legrand, 2019), hydrothermal materials were collected at the LSHF using the hydraulic arm of the Human Operated Vehicle (HOV Nautile 6000). Successively, samples of hydrothermal chimney (Fig. 2a), buoyant hydrothermal fluid (buoyant HF, Fig. 2b), and high temperature hydrothermal fluid (end-members, Fig. 2C) were collected at the Aisics vent site. Upon recovery

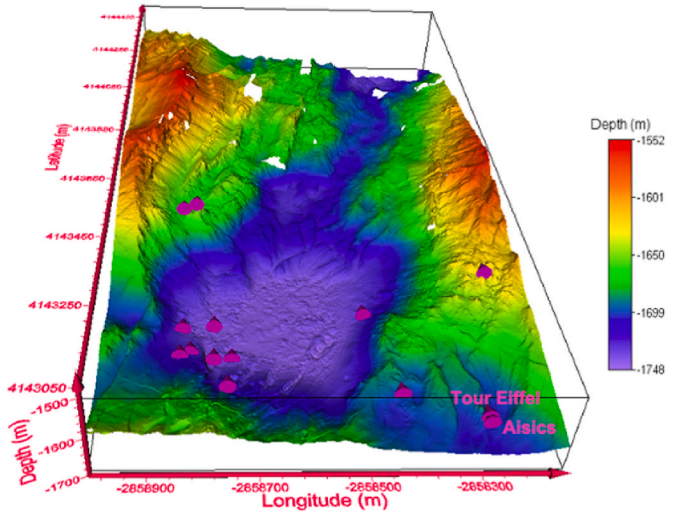

Fig. 1. 3D bathymetric map of the Lucky Strike Hydrothermal Field (LSHF, Ondréas et al., 2009). Active vent locations are indicated by pink 3D cones. (For interpretation of the references to colour in this figure legend, the reader is referred to the Web version of this article.)

of the HOV Nautile on the research vessel, all samples were processed immediately in a shipboard chemical laboratory (Class 100 000, ISO 8).

The anhydrite-bearing top of the Aisics chimney (sample number MOM19_Aisics1, PL, 1939-1, June 12th, 2019) was collected using the bucket arm of the HOV Nautile and then dropped into a decontaminated insulated box (Fig. 2a). Before use, the insulated box was cleaned, disinfected with ethanol, and then filled with sterile distilled water (30 min, 121 °C). To prevent atmospheric contamination before the dive and seawater contamination during the descent and ascent in the water column, the insulated box was opened and closed at depth upon chimney collection. Upon recovery of the HOV Nautile on the research vessel, the hydrothermal chimney was transferred into a sterile mortar under a laminar flow hood, and immediately ground in a controlled anaerobic chamber under an N_2/H_2 (90:10) atmosphere. Due to the friable nature of anhydrite, grinding in a porcelain mortar produced a fairly homogeneous material. The ground chimney was then stored in a glass flask until its introduction into the gas-lift bioreactor tank.

The buoyant HF was collected unfiltered into 5L PVC/DEHP blood bags (Promepla, sterilized by ethylene oxide) via the PLUME fluid pumping system implemented on the HOV Nautile (Fig. 2b). Prior to each dive, the sampling tubes and cannulas of the PLUME device were rinsed with Milli-Q water, then filled with a small volume of Milli-Q water to prevent depression during descent. The temperature sensor, attached to the snorkel of the PLUME device, guided the HOV pilot in collecting the buoyant HF within the mixing gradient at temperature between 100 and 150 °C. All buoyant HF used in this study were collected at the Aisics vent at similar *in situ* temperatures during dives numbered 1939 on June 12th (2 blood bags; samples number MOM19_PL1939-1_PLUME3 and MOM19_PL1939-1_PLUME2), 1941 on June 14th (2 blood bags, > 4L sample number MOM19_PL1941-3_PLUME2 and MOM19_PL1941-3_PLUME3), and 1955 on June 30th (1 blood bag, > 4L sample number MOM19 Aisics PL1955-17_PLUME3). Upon recovery, each filled sterile blood bag was closed and stored at 4 °C in a dark room prior to connection to the gas-lift bioreactor.

Prior to high temperature hydrothermal fluid sampling (Fig. 2c), the fluid temperature was measured *in situ* at 307–309 °C by inserting the HOV high temperature probe into the chimney. A total of eight high temperature hydrothermal fluid were sampled during two dives, on dive 1939 (June 12th, samples M19FLU01 to M19FLU04) and dive 1955 (June 30th, samples M19FLU49 to M19FLU52, Supplementary Material Table S1). These fluids were collected using 200 mL gas-tight titanium syringes. Prior to each dive, gas-tight titanium syringes were washed with diluted hydrochloric acid, then rinsed with ultrapure Milli-Q water. The syringe snorkel was inserted into the chimney and operated individually by the hydraulic arm of the HOV Nautile (Fig. 2c). Upon recovery, the high temperature hydrothermal fluids were extracted from gas-tight titanium syringes, filtered through 0.22 µm Millipore filters, split into distinct aliquots for onboard and onshore analysis, and stored at 4 °C in a dark room. Their chemical composition, analyzed using onshore instrumental and analytical facilities, allows the characterization of pure hydrothermal fluid end-member after extrapolation to Mg-zero prior to its dilution with the surrounding North Atlantic Deep Water (NADW).

For chemical analysis aboard the research vessel, pH, conductivity, salinity, Total Dissolved Solids (TDS), and redox potential (Eh) were measured immediately after fluid extraction using the Consort C562 multi-parameter analyzer. Total Sulfur (TS) and hydrogen sulfide (H_2S) contents were measured with an amperometric micro-sensor (AquaMS, France), connected to both temperature and pH electrodes to establish equilibrium. Dissolved Fe (dFe) concentrations were measured with the HI96721 Iron High Range Photometer (range from 0 to 5 mg/L, Hanna instruments). The instrument was calibrated and validated using Hanna CAL CHECK™ Standards. Prior to each day's measurements, the instrument was zeroed with a blank solution. The measurement accuracy is ±0.04 mg/L ± 2% of reading.

2.3. Gas-lift bioreactor setup

A continuous enrichment culture experiment was conducted aboard the *R.V. Pourquoi Pas?* during the MoMARsat'19 cruise (Sarradin and Legrand, 2019), using a gas-lift bioreactor as shown on Fig. 3 (Callac et al., 2015; Godfroy et al., 2006; Postec et al., 2005b; Postec et al., 2007).

The gas-lift bioreactor was designed to study mineral-fluid-microorganism interactions under controlled conditions approximating the *in situ* environment of diffuse hydrothermal vents. To better represent natural conditions, we followed Callac et al. (2015) by using both the inoculum and culture medium collected directly from a hydrothermal vent. Here, the inoculum was a portion of the Aisics

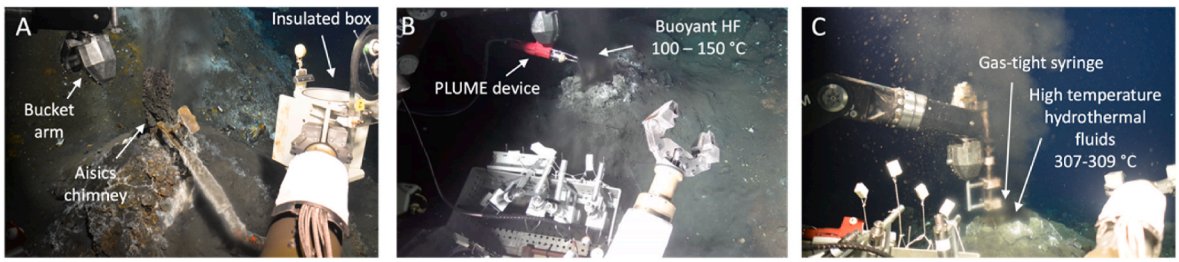

Fig. 2. Chronological overview of scientific operations conducted at Aisics vent site. Snapshots of the HOV Nautile (Sarradin and Legrand, 2019) (A) Collection of Aisics' chimney sample using the bucket arm and an insulated box, (B) Sampling of the buoyant hydrothermal fluids (buoyant HF) with the PLUME device, and (C) Sampling of high-temperature hydrothermal fluids via gas-tight titanium syringe.

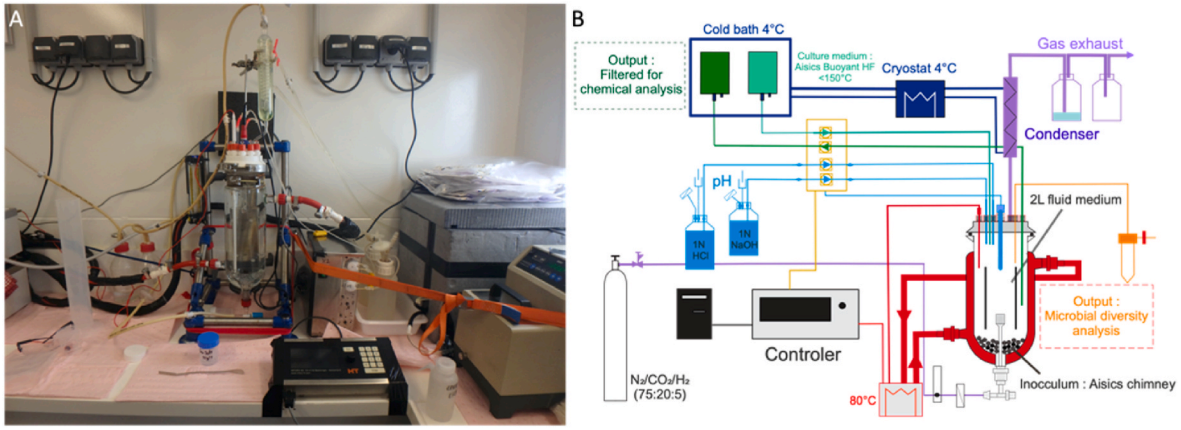

Fig. 3. Set-up of the continuous enrichment culture experiment conducted aboard the *R.V. Pourquoi Pas?* (A) Aboard photograph of the experiment in the laboratory. (B) Schematic illustration of the experimental setup, adapted from Godfroy et al. (2006).

hydrothermal chimney (MOM19_Aisics1), and the culture medium was the buoyant HF collected at the Aisics vent, with temperatures ranging between 100 and 150 °C (see section 2.2).

The bioreactor conditions aimed to support the optimal growth of Aisics microbial communities while enabling continuous monitoring of chemical, microbial, and mineral evolution over time. To do so, stable conditions were maintained: ~80 °C temperature, near-neutral pH (~6.5), atmospheric pressure (1 atm), and an anaerobic environment with continuous gas flow (N_2:CO_2:H_2 at 75:20:5). This setup aligns with methodologies from previous hydrothermal culture experiments (Callac et al., 2015; Godfroy et al., 2000; Postec et al., 2005a). These bioreactor conditions more accurately reflects the environment of diffusive fluids and buoyant hydrothermal fluid near chimneys rather than the immediate interaction zone between high-temperature fluids and chimney structures.

The selected temperature of 80 °C is within the range used in prior bioreactor studies (60–103 °C, Callac et al., 2015; Godfroy et al., 2000; Godfroy et al., 2006; Postec et al., 2005b; Postec et al., 2007; Raven et al., 1992). This temperature is suitable for both thermophilic and hyperthermophilic species typically found in deep-sea hydrothermal environments. While lower than the temperature of pure Aisics hydrothermal fluid (308 °C), the selected temperature more closely approximates conditions in buoyant hydrothermal fluids (100–150 °C) and diffusive vent areas (35–131 °C, Wheeler et al., 2024).

During the experiment, the pH was controlled around 6.5 (dead zone ± 0.2) by adding either 1 N HCl or 1 N NaOH solution (Godfroy et al., 2006). This near-neutral pH aligns with previous hydrothermal bioreactor studies (Callac et al., 2015; Godfroy et al., 2000; Postec et al., 2005a; Postec et al., 2007; Raven et al., 1992) and supports the optimal growth of most species identified in the samples, which thrive at neutral to near-neutral pH (Supplementary Table S3 and references therein). This pH reflects the mixing of hydrothermal fluids with surrounding seawater (pH ~8), as seen in buoyant hydrothermal fluids (pH 6.21) and diffusive vent fluids (pH 5.42–7.22, Wheeler et al., 2024), rather than the more acidic pure hydrothermal fluid (pH < 4.4, Supplementary Table S1).

The anaerobic setup, maintained with a gas mix of N_2:CO_2:H_2 (75:20:5, 10 cm^3/min flow rate), simulate the anoxic conditions of hydrothermal vents. CO_2 and H_2 were chosen as potential carbon sources and electron donors, respectively, with their 1:4 ratio (H_2/CO_2) being standard in microbiology, particularly for culturing methanogens. To ensure safe handling onboard, the H_2 percentage was deliberately kept low (5%), with the remaining 75% consisting of inert N_2. N_2 was selected for its ability to support higher cell densities compared to other inert gases (Raven et al., 1992). This specific gas mixture and proportion (N_2:CO_2:H_2 at 75:20:5) was also used by Callac et al. (2015) in their bioreactor studies.

We operated the bioreactor at 1 atm, a standard choice for hydrothermal culture experiments (Callac et al., 2015; Godfroy et al., 2000, 2006; Postec et al., 2005b; Postec et al., 2007; Raven et al., 1992). While hydrothermal vent environments experience higher pressures, most hyperthermophiles, including those from hydrothermal environments, can be effectively cultured at atmospheric pressure (Godfroy et al., 2006). Although some (hyper)thermophiles are barophilic i.e. their growth rates and protein production is influenced by pressure (Canganella et al., 2000; Erauso et al., 1993; Marteinsson et al., 1999a; Marteinsson et al., 1999b; Miller et al., 1988), operating at 1 atm ensures streamlined cultivation and long-term stability. High-pressure bioreactors, while beneficial for capturing more accurate metabolic profiles under near *in situ* conditions (Foustoukos and Pérez-Rodríguez, 2015), introduce challenges such as variable microbial responses to different pressurization types and potential inhibition from compressed gases (Kelly and Deming, 1988; Nelson et al., 1992). While high-pressure bioreactors (e.g. Foustoukos and Pérez-Rodríguez, 2015) could better mimic *in situ* conditions at diffuse venting, the current stable setup effectively tracks isotopic changes in lithium (Li) and strontium (Sr) without the added complexities of high pressure or pH variations, ensuring direct comparison with previous bioreactor studies.

On June 13th, 2 L of the buoyant HF (sample MOM19_PL1939-1_PLUME3) were introduced into the gas-lift bioreactor tank. After an hour and a half to reach incubation temperature and gas equilibrium, a sample of the culture medium (MOM19_FERM_T-1, Table 1) was filtered through a 0.22 µm Sterivex filter and split into different aliquots for subsequent aboard and onshore chemical analyses. Then, a 150 ml portion of the Aisics hydrothermal chimney (MOM19_Aisics1, inoculum) was introduced into the bioreactor tank; this corresponds to the start of the experiment at T0. By then, we will use the term "fluid medium" to refer to the aqueous phase collected all along the experiment (samples labeled MOM19 _FERM_T1 to T+18 for chemical analysis, Table 1, and MOM19.FerT0 to T18 for microbial analysis, Supplementary Material Table S2). The water/rock ratio is equal to 13 in the gas-lift bioreactor. The chimney was allowed to react with the buoyant HF for an 1 h 15 min before sampling for microbial diversity (MOM19.FerT0). Fifteen minutes after this sample, the continuous injection and withdrawal of fresh fluid began at a rate of 0.025 L/h, maintaining a 2 L culture tank capacity. Throughout the 18-day/432-h experiment, a total of four buoyant HF blood bags (collected on dives PL1939 and PL1941, see section 2.2) were used to maintain the capacity of the culture tank and were connected to the bioreactor at 0 h, 5 h, 120 h, and 288 h, respectively.

The mineralogical composition of the chimney sample was determined by X-Ray Diffraction analysis (XRD) both upon collection and at

Table 1
Geochemical compositions in the gas-lift bioreactor of the buoyant hydrothermal fluid (buoyant HF) before inoculation (MOM19_FERM_T-1), of the fluid medium 24h after inoculation (MOM19_FERM_T1), and of fluid medium sampled at a 48-h intervals until the end of the experiment (MOM19_FERM_T3 to T18).

	Buoyant HF (80 °C)	Fluid medium (80 °C, sample labeled MOM19_FERM_T1 to T18)									
	MOM19_FERM_T-1	T1	T3	T5	T7	T9	T11	T13	T15	**T17**	**T18**
	Before Inoculation	24 h	72 h	120 h	168 h	216 h	264 h	312 h	360 h	**408 h**	**432 h**
Aboard analysis											
pH	6.21	6.66	6.42	6.73	6.60	6.93	6.97	7.15	7.02	7.10	6.52
Total S (mg/L)	190	25	13	22.1	15	17	145	132	54	92	98
H2S (mmol/L)	1.0	0.6	0.1	0.5	0.2	0.4	0.2	1.3	0.8	1.1	1.8
Eh (mV)	3	−92	−18	118	−47	124	129	138	215	46	88
Conductivity (mS/cm)	43.5	46.6	47.3	46.7	46.4	45.1	45.9	44.6	47.1	47.2	47.2
TDS (g/L)	25.4	24.6	27.5	26.5	26.9	26.3	26.6	26	27.4	27.4	27.5
Onshore analysis											
dMg (mmol/L)	28.43	30.79	31.38	30.98	31.47	30.43	30.11	32.33	30.88	32.91	33.9
dCa (mmol/L)	20.37	24.39	23.12	23.01	23.28	24.23	23.94	22.78	22.03	21.5	20.88
dK (mmol/L)	13.97	14.12	14.96	14.1	14.57	16.59	15.65	15.27	14.75	15.94	15.55
dNa (mmol/L)	417.4	429.5	424.7	409.6	419.8	428.1	418	407.2	408.3	421.2	409.6
dFe (µmol/L)	75.1	24.8	20.5	16	21.8	10.8	12.2	16.2	7.6	5.4	4.7
dMn (µmol/L)	65.7	50.2	46.5	45.7	48.3	37.5	90.4	87.7	66.1	46.4	40.8
dSi (mmol/L)	1.68	1.67	1.76	1.82	1.93	1.96	1.94	1.92	2.1	2.32	2.22
dCl (mmol/L)	498.3	511.3	512.1	508.2	505.5	502.3	506.1	509.2	515.8	519.1	520.8
dSO42- (mmol/L)	18.25	24.03	23.22	22.93	22.38	21.95	22.05	22.93	24.65	25.56	26.35
dBa (µmol/L)	1.5	1.4	2.9	2.6	2.4	3.1	4.5	4.3	3	2.4	2.5
dBr (µmol/L)	812	827	823	820	818	812	823	827	832	839	836
dSr (µmol/L)	79	77	75	72	68	85	142	145	133	118	106
87Sr/86Sr	0.707513	0.707488	0.707492	0.707483	0.707404	0.707363	0.707337	0.707439	0.707646	0.707760	0.707794
± 2SE	±0.000004	±0.000004	±0.000004	±0.000004	±0.000004	±0.000005	±0.000005	±0.000004	±0.000005	±0.000005	±0.000004
dLi (µmol/L)	208	162	158	149	166	226	369	387	251	214	179
d7Li (‰)	7.2	4.6	7	6.3	4	7.3	4.6	6.1	7.3	10.3	6.3
Ratios											
dNa/dCl	0.84	0.84	0.83	0.81	0.83	0.85	0.83	0.8	0.79	0.81	0.79
dNa/dLi	2.01	2.66	2.68	2.74	2.52	1.89	1.13	1.05	1.62	1.97	2.28
dMg/dLi	0.14	0.19	0.20	0.21	0.19	0.13	0.08	0.08	0.12	0.15	0.19

the end of the experiment. Upon collection, the inoculum was composed of 93 % of anhydrite ($CaSO_4$), 3 % of pyrite (FeS_2), 2 % halite (NaCl) and 1 % of chalcopyrite ($CuFeS_2$). By the end of the experiment, the inoculum was composed of 91 % of anhydrite, 3 % of pyrite, 3 % halite, and 2 % of chalcopyrite (François, 2021). During the course of the experiment it was not possible to sample the inoculum in the bioreactor.

For chemical analysis (notably elemental and isotope analysis), aliquots of (i) culture medium were extracted before inoculation (MOM19_FERM_T-1, Table 1), and (ii) fluid medium 24 h after the beginning of the experiment and then at 48-h intervals over the following 18 days, resulting in a total of 10 additional samples (samples labeled MOM19_FERM_T1 to T18, Table 1). Each of these 10 samples corresponds to a 24h bioreactor withdrawal, and was collected in 600 ml sterile Terumo blood bags, stored at 4 °C (dark green output bags in Fig. 3B) and then filtered through 0.22 µm Sterivex filter prior to onboard and onshore chemical analyses.

For microbial diversity analysis (bacterial and archaeal diversity), both the chimney sample (sample MOM19_Aisics1) and the buoyant HF fluid (sample M19PL1955_PLUME3 filtered on Sterivex) were stored at -80 °C for subsequent onshore analysis. During the experiment, 50 ml aliquots of the fluid medium were sampled daily (orange falcon on Fig. 3B) and stored at −80 °C for microbial diversity analysis, resulting in a total of 19 samples (samples labeled MOM19.FerT0 to T18, Supplementary Material Table S2). Additionally, 1 ml aliquots stored in a 9 ml Sea water/2% formaldehyde solution and then were filtered through 0.22 µm Nuclepore filters, stained with Sybr Goldfor cell counting with an Axio Imager Z2 Apotome microscope (Carl Zeiss MicroImaging GmbH, Göttingen, Allemagne).

2.4. Microbial diversity analysis

The microbial diversity analysis detailed below was conducted on the buoyant HF (M19PL1955 Plume 3 labeled 19.Ais.100.150 for molecular analysis), the chimney sample (MOM19_Aisics1 labeled M19.Ais1 for molecular analysis), and on eighteen fluid medium samples (samples labeled MOM19.FerT0 to T18, Supplementary Material Table S2). A nested-PCR approach was used to amplify the variable regions V3-V4 of the archaeal 16S rRNA genes. The full-length archaeal 16S rDNA was amplified using the primers A24F-1492R (CGGTTGATCCTGCCGGA; GGCTACCTTGTTACGACT, Lepage et al., 2004; Teske et al., 2002). The PCR products were gel purified and used as a template to amplify the V3-V4 region by using the primers A344F-archaea806R (AYGGGGYGCASCAGGSG; GGACTACVSGGGTATCTAAT, Stahl, 1991; Takai and Horikoshi, 2000). The archaeal 16S rRNA genes libraries were sequenced with Illumina MiSeq at MR DNA (Shallowater, TX, USA). The V3-V4 bacterial 16S rRNA genes libraries were prepared and sequenced with Illumina MiSeq at MR DNA (Shallowater, TX, USA) using the primers whoi341-whoi785R (CCTACGGGNGGCWGCAG; GACTACHVGGGTATCTAATCC, Herlemann et al., 2011). The metabarcoding data were processed using the pipeline SAMBA (https://github.com/ifremer-bioinformatics/samba) which is based on QIIME 2 (Bolyen et al., 2019). Primers and barcode were removed using cutadapt (Martin, 2011), with the following parameters (errorRate = "0.1"; overlap = "5″). Trimming of short reads and low quality sequences, ASVs inference and removal of chimeric sequences were performed using DADA2 (Callahan et al., 2016) with the following parameters (FtrimLeft = "20″ and RtrimLeft = "80″ for *Archaea*; FtrimLeft = "30″ and RtrimLeft = "90″ for *Bacteria*; FmaxEE = "6"; RmaxEE = "6"; minQ = "3"; chimeras = "consensus"). An additional step of ASV clustering has been performed using the dbOTU3 algorithm to avoid an overestimation of the diversity (Olesen et al., 2017). Taxonomic assignment of processed sequences was performed using the SILVA v138 reference database (Quast et al., 2012).

2.5. Elemental and isotopic analysis

All the chemical analyses were conducted at the Observatoire Midi-Pyrénées (Toulouse, France).

The analytical methods used for major dissolved cations (dCa, dK, dMg, dNa, dSi), anions (dCl, dBr, dSO_4), and trace element (dBa, dFe, dMn, dLi, dSr) analyses are detailed in Besson et al. (2014), Leleu (2017), Chavagnac et al. (2018a,b), and Artigue et al. (2022) and will be briefly described below.

Bioreactor samples (samples labeled MOM19_FERM_T-1 to T18, Table 1) were diluted with Milli-Q water 30-fold for dCa, dK, dNa, and 10-fold for dMg and dSi concentration measurements. Other trace element concentrations were measured in pure solutions. All these element concentrations (except for dFe) were measured using an inductively coupled plasma atomic emission spectrometer (ICP-AES) Horiba Ultima2 instrument, with an analytical precision better than 2%. The ICP-AES was calibrated using mono elemental solution and an IAPSO seawater standard solution (OSIL Ltd. UK) diluted 10 to 200-fold with Milli-Q water. The analytical drift was quantified by the standard bracketing method every 8 samples. Detection limits were determined through daily repeated blank solutions (n = 10) at 0.2 µmol/L for dCa, 2 µmol/L for dK, 0.3 µmol/L for dMg, 20 µmol/L for dNa, 0.14 µmol/L for dSi, 0.01 µmol/L for dBa, 0.02 µmol/L for dMn, 0.3 µmol/L for dLi, and 0.01 µmol/L for dSr.

Anion concentrations were measured in 10-fold diluted samples, and determined by anionic chromatography (Dionex ICS-2000) equipped with a specific column for a highly charged matrix (DIONEX IC AS19). The instrument was calibrated with IAPSO seawater standard diluted 10–50 folds with Milli-Q water. The instrument's error is 0.0001 ppm.

For isotopic measurements, all fluids were processed in a clean laboratory to isolate Li and Sr from their matrix using conventional liquid chromatography. For each element, 1 mL of individual fluid samples was evaporated to dryness in a Savillex beaker on a hot plate at 70 °C. The IAPSO and NASS 6 international standards were processed in the same manner and used alongside our samples.

Dissolved Sr was separated from the matrix using Sr-Spec resin (Eichrom, USA) following Pin et al. (2014) protocol. Sr isotopic ratio ($^{87}Sr/^{86}Sr$) was measured using a Thermo Fisher Triton + Thermal Ionization Mass Spectrometer. The $^{87}Sr/^{86}Sr$ ratio was defined as the average values of 150 measurements of ion intensities in the static multi-collection mode. The $^{87}Sr/^{86}Sr$ ratios were corrected from mass fractionation using the $^{86}Sr/^{88}Sr$ normalization ratio of 0.1194. Repeated measurements of the NBS 987 Sr standard gave a mean ratio of 0.710259 ± 0.000013 (2 SD; n = 24; 2SE = 0.000003). The $^{87}Sr/^{86}Sr$ ratios of our samples were corrected from the deviation of the measured NBS 987 to the recommended NBS 987 value of 0.710248.

The $^{87}Sr/^{86}Sr$ ratios of international standards were measured to verify the accuracy of the measurements: 1. IAPSO seawater with a measured value of 0.709174 ± 0.000003 (2SD; n = 4), consistent with published values of 0.709179 ± 0.000007 (2SD; n = 7; El Meknassi et al., 2020), and 2. NASS-6 seawater with a measured value of 0.709174 ± 0.000005 (2SD; n = 3), consistent with published values of 0.709179 ± 0.000014 (2SD; n = 8; Neymark et al., 2014).

Dissolved Li was separated from the NaCl-rich matrix using two steps ion exchange columns made of AGW-X12 200–400 mesh cation resin bed and eluted with 1N HCl (Protocol adapted to NaCl-solution from James and Palmer, 2000). The Li isotopic composition of each fluid sample was measured on a Thermo Fisher Triton + Thermal Ionization Mass Spectrometer at the Observatoire Midi-Pyrénées. Additional information regarding sample loading and mass spectrometer setup can be found in Artigue et al. (2022). The $^{7}Li/^{6}Li$ ratios are expressed in the $\delta^{7}Li$ ‰ notation relative to the IRMM-16 Li standard (Li_2CO_3) at similar Li concentration. Repeated measurements of the IRMM-16 standard gave a mean $^{7}Li/^{6}Li$ ratio of 12.082 ± 0.012 (2SD; n = 17), an internal precision of 0.25 ‰ (2SE) and an external precision of 1.03 ‰ (2SD; n = 17). The accuracy of our technique was verified against the measured ratios

of the international IAPSO seawater standard with a measured value of +29.5 ± 0.2 ‰ (2SE), consistent with published values of +30.8 ± 0.1 ‰ (2SE, with external precision ≤1‰, Rosner et al., 2007).

2.6. Geochemical modeling

Geochemical modeling was performed with the PHREEQC software package developed by USGS (Graphical User Interface Version 3, www.usgs.gov/software/phreeqc-version-3, Parkhurst and Appelo, 2013). PHREEQC can be used as a speciation program, particularly to calculate the distribution of aqueous species, and the possibility of mineral dissolution/precipitation. To perform these speciation calculations, PHREEQC requires the major elements total concentrations of the solution (user input) and the specific equilibrium constants from the PHREEQC databases. The saturation state of the fluid regarding to minerals is given by its saturation index (SI), which is calculated as the logarithm of the chemical activities of the dissolved ions (ion activity product, IAP) over their solubility constant (K). The possibility of a mineral to dissolve or precipitate is characterized by either undersaturation (SI < 0) or oversaturation (SI > 0).

In this study, the PHREEQC program was used along with the "llnl.dat" database (Johnson et al., 1992). This database provides logarithms of equilibrium constants (log K) along with thermodynamical data available up to 300 °C. The speciation modeling was run twice on the buoyant HF: first at its *in situ* temperature (126 °C), and then after reaching the incubation temperature (80 °C) and gas equilibrium of the gas-lift bioreactor. Subsequently, it was run on each aliquot of fluid medium extracted after inoculation from the gas-lift bioreactor (10 samples, MOM19_FERM_T1 to T18). The chemical composition of the fluids was input as total concentrations of all previously analyzed chemical elements. To model the continuous gaseous flush of N_2:CO_2:H_2, thermodynamic equilibrium was established between the fluid and a gas phase at a total pressure of 1 atm and at the N_2:CO_2:H_2 proportions (75:20:5) of the gas-lift bioreactor setup.

In the modeling, the oxidation potential was calculated regarding the H_2S/SO_4^{2-} redox couple. Li and Sr aqueous species distribution was calculated as well as the saturation indices (SI) for both the buoyant HF and the fluid medium throughout the entire duration of the bioreactor experiment.

3. Results

3.1. Geochemistry of pure hydrothermal fluids

The geochemical features of the high temperature hydrothermal fluids collected during MoMARsat'19 cruise are reported in Supplementary Material Table S1. High temperature hydrothermal fluids exhibit pH values at 25 °C ranging between 3.58 and 4.40 (Chavagnac et al., 2023), and chemical enrichment in dissolved Ca, K, Si, Fe, Mn, Si, and Li (dCa, dK, dSi, dFe, dMn, dLi) compared to seawater. Since pure hydrothermal fluid should be totally dMg-depleted, the end-member composition is obtained by linear extrapolation to zero-Mg of the least-square regression method (Von Damm et al., 1998). The result is similar to previous end-member chemical features obtained at this site (Chavagnac et al., 2018a,b; Leleu, 2017). However, H_2S concentrations of 4.1–11.9 mmol/L, are much higher than previous values of 2–4 mmol/L (Charlou et al., 2000; Chavagnac et al., 2018; Pester et al., 2012; Von Damm et al., 1998).

3.2. Elemental and isotopic composition of bioreactor fluid medium

The elemental and isotopic composition of the buoyant HF, and all fluid medium extracted from the gas-lift bioreactor are reported in Table 1 and are shown in Fig. 4.

The pH of the buoyant HF in the bioreactor before inoculation is 6.21. Throughout the experiment, pH values ranged between 6.42 and 7.15 (Table 1). Dissolved Na and dCl vary from 407 to 430 mmol/L and 502–521 mmol/L, respectively, and the dNa/dCl ratios show little

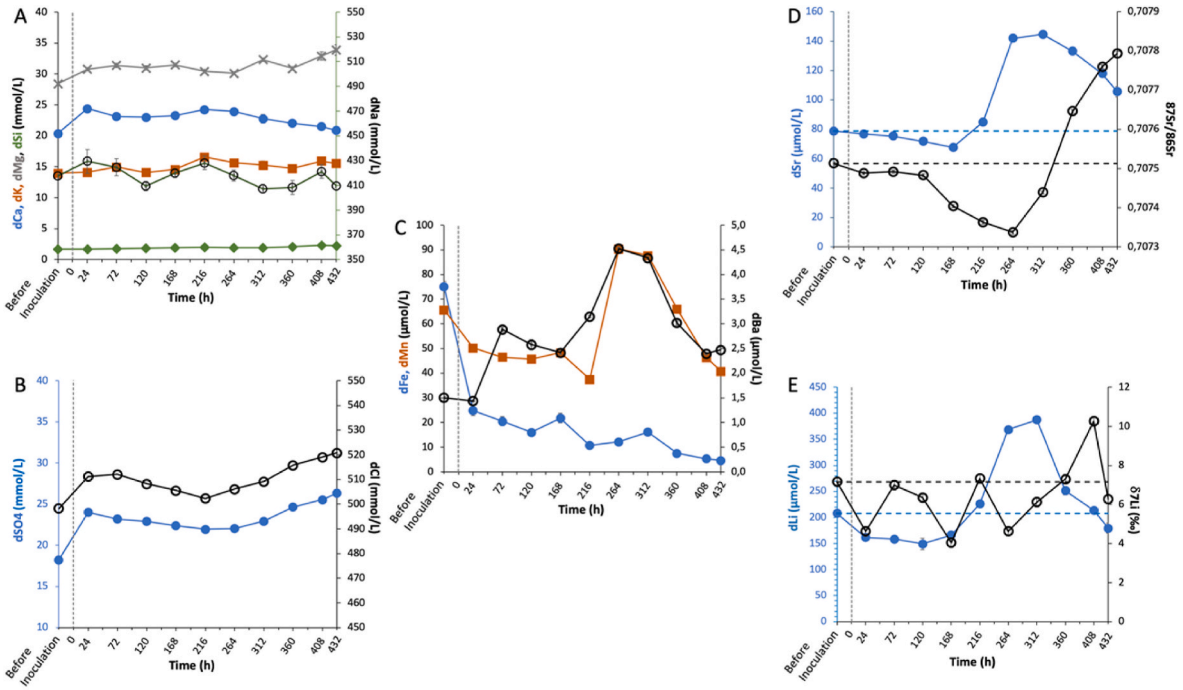

Fig. 4. Temporal evolution of the geochemical composition in the gas-lift bioreactor of the buoyant hydrothermal fluid (Buoyant HF) before inoculation, and of the fluid medium 24h after inoculation and at 48-h intervals until the end of the experiment. The start of the experiment i.e. inoculation time is indicated at 0 h. (A) Major cation concentrations, (B) Major anion concentrations, (C) dFe, dMn, dBa concentrations, (D) dSr concentrations and $^{87}Sr/^{86}Sr$ ratios, and (E) dLi concentrations and δ^7Li ‰ values. For (D) and (E), horizontal lines denote the initial values, aiding in visualizing fluctuations from the collection time to the end of the experiment. All data are plotted with their respective uncertainties.

variation at 0.79–0.85 compared to a standard seawater ratio of 0.86 (Millero et al., 2008). Between the sampling of the buoyant HF in the gas-lift bioreactor before inoculation (MOM19_FERM_T-1, Table 1) and the first sampling of the fluid medium for chemical analysis 24 h after inoculation (MOM19_FERM_T1, Table 1), element concentrations exhibit various trends. Concentrations of dNa, dK, dCl, dBr, dBa, and dSr remain fairly constant, while dSO_4, dCa, and dMg increase by up to 32%, 20%, and 8%, respectively. Conversely, concentrations of dFe, dMn, and dLi decrease by 67%, 24%, and 22%, respectively (Fig. 4). Then, from 24 h to 168h, element concentrations are overall constant, with slight reductions of dCa, dSO_4, dMn, and dSr concentrations by up to 5%, 7%, 4%, and 12%, respectively (Fig. 4A, B, and D). Between 168 h and 264 h, major element concentrations remain stable; however, all trace element concentrations, except dFe, doubled (dMn, dBa, dSr, and dLi). Subsequently, from 264 h to the end of the experiment, trace elements, along with dCa, decreased progressively: dMn by 55%, dLi by 51%, dBa by 45%, dSr by 26%, and dCa by 13%, while dSO_4 and dMg concentrations increased by up to 20% and 13%, respectively. Regarding the variability in dFe, it continuously decreases over time, by up to a factor of 5 by the end of the experiment (Fig. 4C).

The $^{87}Sr/^{86}Sr$ ratio of the gas-lift bioreactor culture medium before inoculation was measured at 0.707513 ± 0.000004 (MOM19_FERM_T-1, Table 1). From this sampling time to 24 h after the experiment start, the $^{87}Sr/^{86}Sr$ ratio of the fluid medium decreases down to 0.707488, remaining relatively stable until 120 h, before decreasing to its minimum value of 0.707337 at 264 h. From 264 h onwards, the $^{87}Sr/^{86}Sr$ ratios continuously increase reaching a maximum value of 0.707794 by the end of the experiment (Fig. 4d). Regarding the Li isotopic composition, the δ^7Li values show a large variation between +4.0 and + 10.3 ‰ with a median value of +5.5 ‰ without any specific temporal evolution (Fig. 4e).

3.3. PHREEQC geochemical modeling: saturation state and aqueous speciation

PHREEQC geochemical modeling is controlled by the physico-chemical conditions of the experiment. It allows a thermodynamic diagnosis of the reactivity in the bioreactor fluid medium throughout the experiment, but doesn't account for kinetics. The mineral saturation indexes and element species abundances calculated by PHREEQC are presented in Table 2. Considering the observed minerals in the inoculum, thermodynamic calculations evidence the continuous undersaturation state of the medium fluid regarding anhydrite ($CaSO_4$) throughout the experiment, suggesting anhydrite dissolution. However, the saturation indices of sulfides such as pyrite (FeS_2) and chalcopyrite ($CuFeS_2$), as well as oxides such as hematite (Fe_2O_3), calcite ($CaCO_3$) and other carbonates, and even barite ($BaSO_4$) are all positive. This suggests either their stability in the fluid medium (for chalcopyrite) or their potential precipitation. Note that the continuous flushing of N_2: CO_2:H_2 gaseous phase ensures anaerobic conditions which preserve sulfur mineralization.

Dissolved Sr speciation in solution is essentially composed of Sr^{2+}, $SrCl^+$ and $SrSO_4$ species at ~85 %, ~10 % and ~4 %, respectively. The $SrCO_3$ species is present at the percent level when pH of the fluid medium is close to 7 or above. Dissolved Li speciation consists of 98 % of Li^+ species with a contribution of ~1 % for LiCl and $LiSO_4^-$ species.

3.4. Microbial diversity evolution in the bioreactor

The microbial diversity (bacterial and archaeal diversity) found throughout the experiment is presented in Fig. 5 and in Supplementary Material Table S2. These data show the relative abundance of the most representative taxa based on their sequence proportions. It is important

Table 2
Mineral saturation indexes and element species abundances of (i) the buoyant hydrothermal fluid (Buoyant HF) at *in situ* temperature (126 °C), (ii) the buoyant HF after reaching incubation temperature (80 °C) and gas equilibrium (MOM19_FERM_T-1), and (iii) the fluid medium 24 h after inoculation (MOM19_FERM_T1), and then at 48 h intervals until the end of the experiment (MOM19_FERM_T3 to T18). All values were calculated using PHREEQC aqueous geochemical modeling.

	Buoyant HF (126 °C)	Buoyant HF (80 °C)	Fluid medium (80 °C, samle labeled MOM19_FERM_T1 to T18)									
	MOM19-FERM T-1	MOM19-FERM T-1	T1	T3	T5	T7	T9	T11	T13	T15	T17	T18
	In situ	Before Inoculation	24 h	72 h	120 h	168 h	216 h	264 h	312 h	360 h	408 h	432 h
Mineral saturation index (SI)												
Anhydrite (CaSO4)	0.10	−0.30	−0.13	−0.17	−0.18	−0.18	−0.17	−0.19	−0.19	−0.18	−0.19	−0.16
Gypsum (CaSO4:2H2O)	−0.58	−0.63	−0.46	−0.50	−0.51	−0.51	−0.50	−0.52	−0.52	−0.51	−0.53	−0.49
Barite (BaSO4)	−0.38	−0.02	0.06	0.35	0.31	0.26	0.37	0.54	0.53	0.42	0.32	0.34
Pyrite (FeS2)	8.15	9.57	7.58	7.00	7.31	7.10	6.94	8.55	8.65	7.60	7.81	7.88
Pyrrhotite (FeS)	3.18	2.79	1.50	1.17	1.49	1.18	1.13	2.33	2.35	1.68	1.81	1.30
Hematite (Fe2O3)	3.68	1.04	0.54	0.55	0.79	0.37	0.25	0.82	0.83	0.49	0.33	−1.22
Quartz (SiO2)	0.09	0.48	0.47	0.49	0.50	0.54	0.54	0.52	0.52	0.56	0.59	0.60
Strontianite (SrCO3)	−0.12	0.04	0.20	0.27	0.67	0.07	0.56	1.38	1.17	1.33	1.45	0.20
Calcite (CaCO3)	1.05	0.88	1.12	1.17	1.58	1.02	1.43	1.99	1.76	1.93	2.08	0.91
Rhodochrosite (MnCO3)	−0.20	0.03	0.07	0.12	0.53	−0.02	0.27	1.23	1.00	1.06	1.08	−0.16
Species abundances (%)												
Lithium												
Li+	98.0	98.2	98.0	98.0	98.0	98.1	98.1	98.1	98.0	97.9	97.9	97.9
LiCl	1.7	1.1	1.1	1.1	1.1	1.1	1.1	1.1	1.1	1.1	1.1	1.1
LiSO4-	0.4	0.7	0.9	0.9	0.9	0.8	0.8	0.9	0.9	1.0	1.0	1.0
LiOH	0.0	0.0	0.0	0.0	0.0	0.0	0.0	0.0	0.0	0.0	0.0	0.0
Strontium												
Sr2+	82.3	87.4	86.5	86.5	86.3	86.8	86.8	85.9	86.1	85.3	84.9	85.9
SrCl+	16.1	9.0	9.0	9.1	9.1	9.0	8.9	8.9	9.0	9.1	9.0	9.2
SrSO4	1.5	3.5	4.4	4.2	4.3	4.1	4.0	4.1	4.2	4.7	4.7	4.7
SrCO3	0.1	0.1	0.1	0.1	0.4	0.1	0.3	1.0	0.6	1.0	1.4	0.1
Sulfide S(-II)												
HS-	70.8	65.5	69.9	71.7	80.3	67.8	76.9	86.9	83.8	86.6	88.8	66.5
H2S	29.1	34.5	30.1	28.3	19.6	32.2	23.1	13.1	16.2	13.4	11.2	33.5
Sulfate S (+VI)												
MgSO4	58.5	37.3	36.6	37.4	37	38	36.6	35.3	37.7	35.6	36.1	39.0
SO42-	26.1	39.0	38.9	38.6	39.3	38.2	38.8	40.2	39	40.7	40.3	38.3
NaSO4-	9.3	17.0	17.1	16.9	16.7	16.6	17.1	17.2	16.4	17.0	17.2	16.1
CaSO4	5.2	5.7	6.5	6.1	6.1	6.2	6.4	6.1	5.9	5.7	5.2	5.5
KSO4-	0.9	0.9	0.9	0.9	0.9	0.9	1.0	1.0	1.0	1.0	1.0	1.0

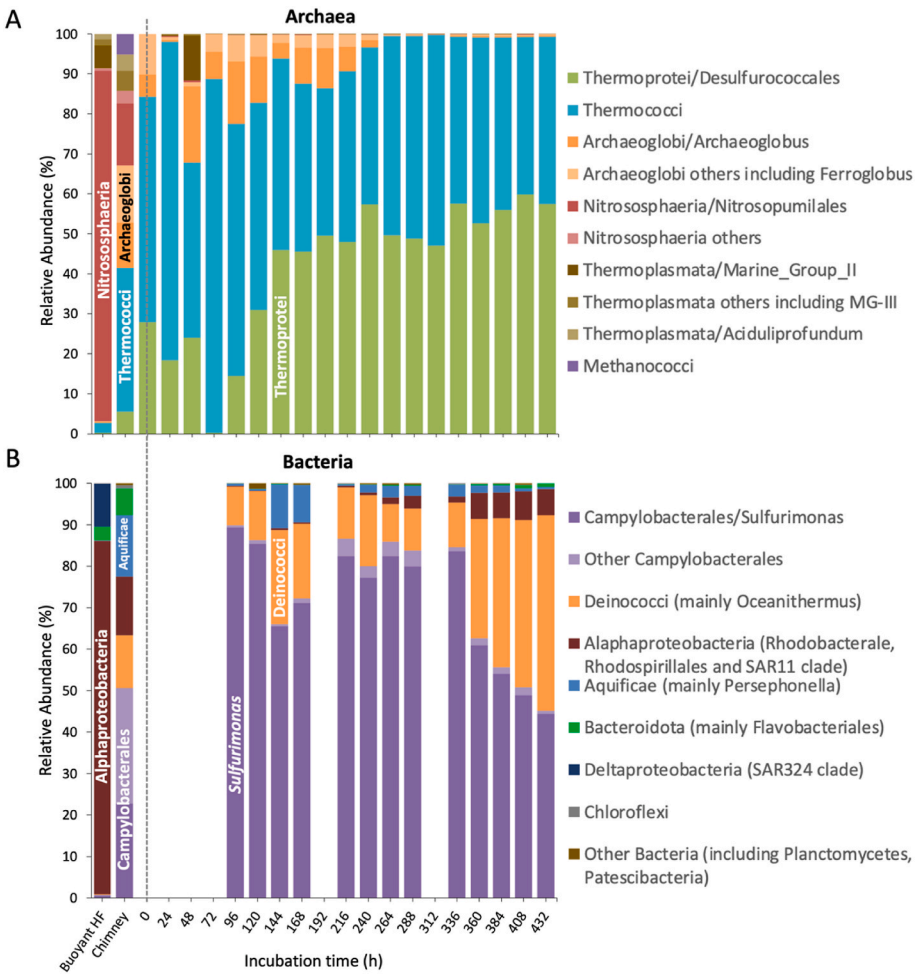

Fig. 5. Barplots presenting the relative abundance of (A) Archaea and (B) Bacteria enriched in the continuous culture over the incubation time (x-axis, hours). The microbial diversity in both the Aisics chimney sample (used as the inoculum) and the buoyant hydrothermal fluid (buoyant HF, used as the culture medium) is also presented. All taxa names are in the legend, with main taxa labeled on corresponding bars for clarity.

to note that these data indicate the detected archaeal and bacterial taxa for each incubation time, thus conveying semi-quantitative variations.

The cell counts of microbial communities show an overall increase throughout the experiment, reaching 2×10^5 cell/mL at 120 h, then varying around 6×10^6 cell/mL at 240 h before reaching a maximum of 8.5×10^6 cell/mL at 360 h, then cells concentration slightly decrease to reach 4×10^6 cells/mL at the end of the experiment (François, 2021). At all sampling times, archaeal sequences were detected, whereas no bacterial sequences were obtained until 96 h, at 192 h, and at 312 h. This could be due to the sequencing reaction failing because of too low bacterial abundance, or the number of sequences being too low once contaminants were removed for bacterial diversity analysis. Due to the length of 16S RNA gene sequences obtained using illumina sequencing, identification of enriched microorganisms was possible up to the order level for Archaea and up to the genus level for some Bacteria.

The archaeal diversity within the buoyant HF is mainly dominated by the class Nitrososphaeria (88%), with the *Nitrosopumulales* being the most represented order (Fig. 5a–Supplementary Material Table S2). Nitrososphaeria was also detected in the chimney sample but at significantly lower abundance (19%) compared to the buoyant HF. Within the chimney, Thermococci is the most abundant class (36%), followed by the Archaeoglobi class (26%) which includes *Archaeoglobus* and other genera such as *Ferroglobus*. Additionally, the class Thermoprotei, with the *Desulfurococcales* being its most represented order and the class Methanococci were detected in low abundance in the chimney (6% and 5%, respectively, Fig. 5a). The class Thermoplasmata, including the genus *Aciduliprofundum* and Marine Group-III (MG-III), was detected at a few percent's in both buoyant HF and chimney samples (3% and 9%, respectively), while the Thermoplasmata Marine Group-II (MG-II) was only detected in the buoyant HF (6%). Regarding bacterial diversity, the buoyant HF is largely dominated by the class Alphaproteobacteria (85%) including the orders *Rhodobacterales* and *Rhodospirillales*, and the SAR11 clade (Fig. 5b). Additionally, the class Deltaproteobacteria (SAR324 clade) and the Phylum Bacteroidota (mainly *Flavobacteriales* order) are also present in the buoyant HF, albeit at low (10%) and very low abundances (3%), respectively. By contrast, the chimney sample display higher bacterial diversity with the *Campylobacterales* order (including *Sulfurimonas* genus and other *Campylobacterales*) being dominant (51%), and classes such as Aquificae (mainly *Persephonella* genus), Deinococci (mainly *Oceanithermus* genus), Alphaproteobacteria, and Bacteroidota being detected at 15%, 13%, 14%, 6%, respectively. In the fluid medium, Thermococci and Themoprotei are the most abundant archaea classes, except at 72 h where no Thermoprotei were detected. Archaeoglobi represent between 3% and 22% of the Archaeal diversity during the first 240 h (except at 24h) but afterward decrease to less than 1% until the end of the experiment. Regarding bacterial diversity, the *Campylobacterales* genus *Sulfurimonas* dominates until 360 h (between 61% and 89%), after which it shares prevalence with the Deinococci class (mainly *Oceanithermus*). Both Aquificae (mainly *Persephonella*) and Alphaproteobacteria classes were detected in almost all samples at very low abundance. However, Aquificae peaked at approximately 10% at 144 and 168 h and Alphaproteobacteria reached ~6% from 360 h to the

end of the experiment (Fig. 5b–Supplementary Material Table S2).

4. Discussion

In the gas-lift bioreactor, the chemical and isotopic composition of the fluid medium results from interactions with minerals, microorganisms (archaea and bacteria) and gases (bioreactor setup conditions). In section 4.1, we will characterize the collected materials, i.e., the Aisics chimney (used as the inoculum) and the buoyant HF (used as the culture medium), along with their microbial diversity. Once these materials are introduced into the gas-lift bioreactor, the experiment starts. In section 4.2, we will discuss how the elemental and isotopic chemical composition of the fluid medium respond to the evolution of microbial diversity and the mineral precipitation/dissolution processes.

4.1. Characterization of the collected materials

The buoyant HF was collected *in situ* between 100 and 150 °C (François, 2021). Both the buoyant HF and the end-member high temperature hydrothermal fluid exhibit enrichment in dCa, dK, dSi, dFe, dMn, dLi compared to seawater (Table 1 and S1, Leleu, 2017; Millero et al., 2008). The measured chemical composition of the buoyant HF can be modeled by an adiabatic and conservative mixing between Aisics hydrothermal end-member and NADW. Major cation and anion concentrations correspond to a contribution of 35–44 % of hydrothermal end member and a temperature range of 110–141 °C, consistent with the in-situ temperature of buoyant HF collection (100–150 °C, Supplementary Material Fig. S1). The buoyant HF is characterized by a $^{87}Sr/^{86}Sr$ ratio of 0.707513 ± 0.000004 and a δ^7Li value of +7.2‰. While the Sr isotopic signature is fully coherent with those obtained through conservative mixing of 35–44% of the hydrothermal end-member with NADW, and the Li isotopic value corresponds to a 54% end-member contribution and a temperature of 170 °C (Supplementary Material Fig. S1). Contrarily to cations and anions, the end-member Sr and Li isotopic values were taken from AISICS end-member measurements between 2013 and 2015, as the 2019 values are not available (Artigue et al., 2022; Chavagnac et al., 2018a,b; Leleu, 2017). Thus, this discrepancy might be attributed to a slight change in the Aisics end-member δ^7Li value in 2019, or to potential fractionation processes during mixing between end-member and seawater. Indeed, while the instrument analysis of the $^{87}Sr/^{86}Sr$ ratio eliminates mass-dependent Sr isotope fractionation occurring before or during the analysis (Andrews et al., 2016), the δ^7Li values are affected by Li isotopes fractionation notably controlled by minerals precipitation/dissolution (Hindshaw et al., 2019; Vigier et al., 2008; Wang et al., 2023).

The chimney sample (inoculum) is mainly composed of anhydrite (at 93%) which has a retrograde solubility at temperatures below 150 °C (Bischoff and Seyfried, 1978). Sulfur bearing minerals, pyrite and chalcopyrite, are present in smaller proportions (at 1 and 3%, respectively). These minerals can provide element and energy for sulfur or sulfate reducer or oxidizer microorganisms. Indeed, archaeal and bacterial development depends not only on the physico-chemical state of the buoyant HF or inoculum but also on the bioavailable energy sources provided through chemical components releasing and/or accepting electrons.

The microbial diversity (bacteria and archaea) is summarized in Supplementary Material Table S3, along with their origins in the gas-lift bioreactor (buoyant HF or chimney), their occurrence or absence in the fluid medium, optimal growth temperature, and main known metabolism.

The most abundant archaeal class found in the buoyant HF is Nitrosophaeria (mainly *Nitrosopumulales*), which is also present in the inoculum but at a lower abundance (Fig. 5a–Supplementary Material Table S2). Nitrosophaeria are commonly retrieved in deep sea water and were already detected at hydrothermal environments (Takai et al., 2004; Teske et al., 2021). At LSHF they were identified in microbial mats (associated or not with mussel assemblages) either located at the base of the Tour Eiffel vent at LSHF (<10°C, Crépeau et al., 2011; Rommevaux et al., 2019) or at diffuse venting at the same site (40–55°C, Astorch-Cardona et al., 2023). However, Nitrosophaeria growth appears to be inhibited by acidic, anaerobic and high temperature conditions typical of hydrothermal environments, favoring instead aerobic, neutrophilic, and mesophilic seawater conditions (Supplementary Material Table S3, Baker et al., 2012; Könneke et al., 2005; Qin et al., 2016; Qin et al., 2017; Teske et al., 2021). As a result, although Nitrosophaeria are abundant in the buoyant HF, the anaerobic, high temperature (80 °C) conditions of the bioreactor are likely unfavorable for its development.

The Thermoplasmata class was detected at a few percents in both the buoyant HF and the chimney sample. This class includes the genus *Aciduliprofundum*, as well as marine groups MG-II and MG-III, with MG-II only detected in the buoyant HF (Fig. 5a–Supplementary Material Table S2). The presence of *Aciduliprofundum*, which is commonly found in deep-sea vents, is unsurprising; however, MG-II and MG-III are generally low in abundance in the deep sea and are rarely present in hydrothermal chimneys (François, 2021; Haro-Moreno et al., 2017; Rinke et al., 2019; Zhang et al., 2015). The bioreactor near-neutral pH may inhibit the growth of the thermoacidophilic *Aciduliprofundum*, while its high temperature (80 °C) is unfavorable for the mesophilic marine groups MG-II and MG-III (Supplementary Material Table S2, Reysenbach et al., 2006; Santoro et al., 2019).

In contrast, the most abundant archaeal classes in the chimney sample, i.e. Thermococci and Archaeoglobi, and to a lesser extent Thermoprotei are well-suited to the bioreactor conditions (Figs. 5a and 6a). The presence of these taxa in the chimney sample is consistent with previous studies of deep-sea hydrothermal environments, notably at the Tour Eiffel site of the LSHF (Huber et al., 1997, 2006; Reysenbach et al., 2000; Rommevaux et al., 2019). These taxa, described as anaerobes (or facultative anaerobes), (hyper)thermophilic, thrive in slightly acidophilic to alkaline conditions, aligning well with the anaerobic, high temperature, and near-neutral pH environment of the bioreactor (Supplementary Material Table S3 and reference therein). Engaging in sulfur and iron cycling, these taxa may significantly influence fluid chemistry. For instance, the Archaeoglobi class includes *Archaeoglobus* and other genera such as *Ferroglobus* (Fig. 5a–Supplementary Material Table S2). *Archaeoglobus* genus can reduce sulfate, sulfite, or thiosulfate compounds to H_2S using organic substrate and/or H_2 as electron donors (dissimilatory sulfate reduction, Barton et al., 2014; Burggraf et al., 1990; Hartzell and Reed, 2006; Liu et al., 2012; Mori et al., 2008; Offre et al., 2013). *Ferroglobus* genus is an Fe(II) oxidizer or an Fe(III) reducer (Hafenbradl et al., 1996; Tor and Lovley, 2001). Both the Thermoprotei (primarily *Desulfurococcales* order), and the Thermococci (including the *Thermococcales* order), have species involved in the sulfur cycle. Some *Desulfurococcales* growth autotrophically by oxidizing hydrogen using sulfur, nitrate, or nitrite compounds as electron acceptor, and CO_2 as a carbon source. Organotrophic growth can also occur through aerobic respiration, anaerobic sulfur respiration with organic compounds as electron donors, or fermentation of organic compounds with elemental sulfur as the electron acceptor (Huber and Stetter, 2006; Liu et al., 2012). Note that some members of *Desulfurococcales* cannot use elemental sulfur or sulfur compounds (Huber and Stetter, 2006). *Thermococcales* species are organotrophic thermophiles that can also growth through fermentation of organic compounds with or without elemental sulfur (Bertoldo and Antranikian, 2006; Liu et al., 2012). While elemental sulfur stimulates the growth of *Thermococcales*, it is not always essential, and some thrive without elemental sulfur. In the presence of elemental sulfur, it is reduced to H_2S; in its absence, H_2 is produced by proton reduction (Schut et al., 2014). Therefore, the metabolic characteristics of taxa from Thermococci, Archaeoglobi, and Thermoprotei make them particularly well-suited to the bioreactor's continuous N_2:CO_2:H_2 gas flow and its mineral composition, which includes anhydrite and sulfur-bearing minerals like pyrite and

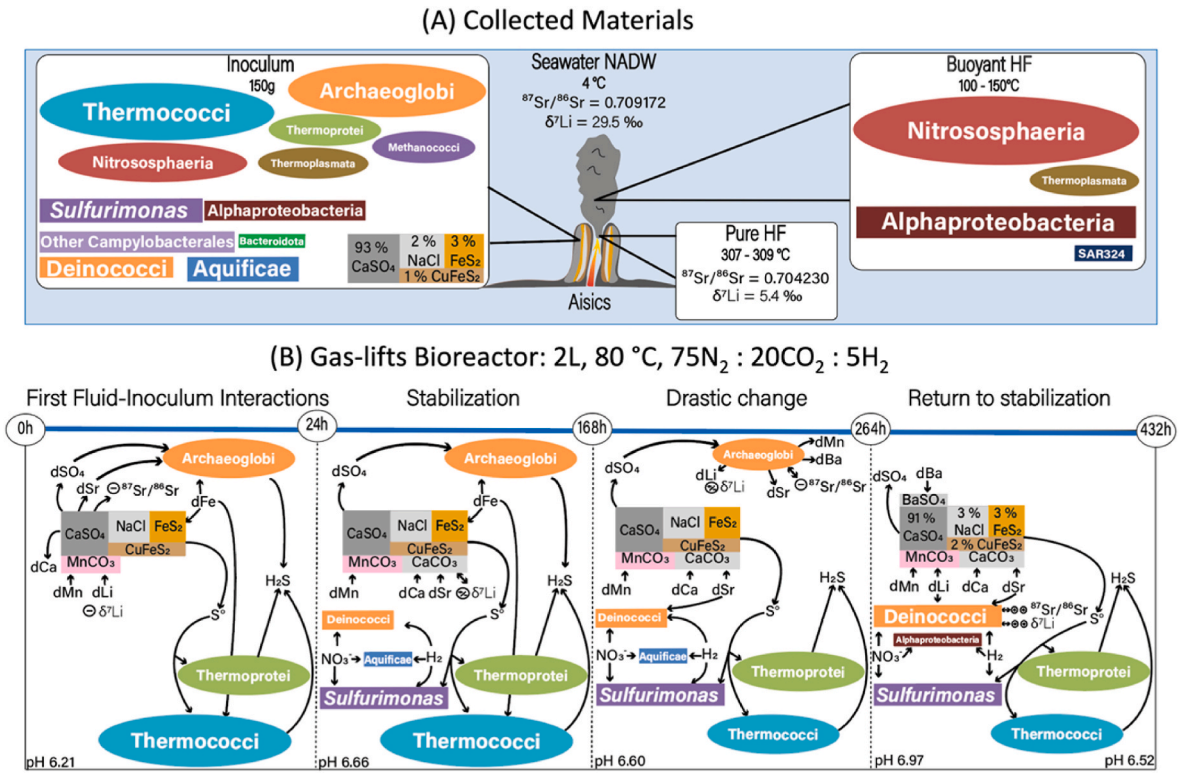

Fig. 6. Conceptual model illustrating (A) the mineral, microbial, and chemical composition of the collected materials: the high-temperature pure hydrothermal fluid (Pure HF), the buoyant hydrothermal fluid (Buoyant HF, culture medium), and the Aisics chimney (Inoculum). (B) The model showcases the impacts of mineral-fluid-microorganism interactions on the evolution of the fluid medium within the gas-lift bioreactor across four distinct time intervals: first fluid-inoculum interactions, stabilization, drastic change, and return to stabilization, as detailed in the Discussion.

chalcopyrite.

Methanococci were detected in the chimneys samples at a low abundance (5%). Methanococci are methanogenic archaea that produce methane from H_2 and CO_2. Although commonly found in hydrothermal vents, this is their first detection in the Lucky Strike chimneys (Flores et al., 2011; Jeanthon et al., 1999; Jones et al., 1983, 1989; Whitman and Jeanthon, 2006).

The most abundant bacterial class identified in the buoyant HF is Alphaproteobacteria, including the orders *Rhodobacterales* and *Rhodospirillales*, and the SAR11 clade (Fig. 5B–Supplementary Material Table S2, Garrity et al., 2005). This class is also present to a lesser extent in the chimney sample, probably originating from the surrounding seawater. Alphaproteobacteria are ubiquitously distributed in the marine environment (Morris et al., 2002; Rappé et al., 2002) and notably found in black smoker chimneys (Voordeckers et al., 2008), microbial mats from the LSHF (Astorch-Cardona et al., 2023; Crépeau et al., 2011) and sediments (Cerqueira et al., 2017). This is consistent with their abundance in our collected buoyant HF. Additionally, SAR324, an uncultivated clade of Deltaproteobacteria, is only present in the buoyant HF (Figs. 5b and 6a). Known for its metabolic flexibility (Sheik et al., 2014; Swan et al., 2011; Wright et al., 1997), SAR324 clade can thrive in the full water column (Boeuf et al., 2021) and marine environments in the vicinity of hydrothermal sites (Dick et al., 2013; Dick and Tebo, 2010; François, 2021). This aligns well with its presence in our buoyant HF. Some Bacteroidota (mainly *Flavobacteriales* order) were detected at a few percents in both the buoyant HF and the chimney. Species of the *Flavobacteriales* order are primarily known to inhabit surface cold water environments (Gómez-Pereira et al., 2010); however, one species was isolated from a biofilm on the surface of a black smoker chimney on the Arctic Mid-Ocean Ridge (Wissuwa et al., 2017). This suggests that, while uncommon, their presence in hydrothermal samples is not unprecedented. As with archaeal diversity, bacterial diversity in the chimney sample is greater than in the buoyant HF (Fig. 5). In the chimney sample, the bacterial abundance is dominated by *Campylobacterales* with the *Sulfurimonas* genus, and other *Campylobacterales*. Then, the remaining of the bacterial diversity is shared between Alphaproteobacteria, Aquificae, Deinococci, and with a lower abundance Bacteroidota (mainly *Flavobacteriales*, Figs. 5b and 6a). All of these taxa have been previously found in deep-sea hydrothermal environments (Li et al., 2020; Miroshnichenko et al., 2003; Molari et al., 2023; Reysenbach et al., 2000; Sievert et al., 2000; Waite et al., 2017; Zeng et al., 2021; Zhang et al., 2016). *Sulfurimonas* and other *Campylobacterales* and Aquificae (mainly *Persephonella*) were specifically identified at the LSHF and at the Aisics chimney of the Tour Eiffel site (François, 2021; François et al., 2021; Mino et al., 2017; Rommevaux et al., 2019). The *Sulfurimonas* genus is described as mesophilic chemolithoautotroph bacteria that grow at an optimum pH range from 4.5 to 8.6, relying on the presence of hydrogen, elemental sulfur or thiosulfate as the sole energy source, carbon dioxide as the sole carbon source, and ammonium or nitrate as the sole nitrogen source (François et al., 2021; Hu et al., 2021; Supplementary Material Table S3, Takai et al., 2006; Zeng et al., 2021). Despite the high temperature, the bioreactor's near-neutral pH and available energy, carbon, and nitrogen sources may support *Sulfurimonas* activity. Bacteria from the Aquificea class (mainly *Persephonella*) are thermophilic and grow in microaerophilic conditions, oxidizing hydrogen, elemental sulfur, or thiosulfate using oxygen as an electron acceptor. However, in anaerobic conditions, they can adapt by using hydrogen as electron donor and nitrate as electron acceptor, performing anaerobic nitrate reduction (François et al., 2021; Supplementary Material Table S3, Reysenbach et al., 2001; Zeng et al., 2021). A novel strain of the *Persephonella* genus, *Persephonella atlantica* sp. nov. (strain MO1340^T) was isolated from the Aisics chimney (François, 2021; François et al., 2021). This finding suggests that certain *Persephonella* species are well-suited to the anaerobic conditions of the bioreactor, where hydrogen and nitrate are

available to support their growth. Deinococci (mainly *Oceanithermus* genus) were detected in the chimney samples (Fig. 5b). The thermophilic *Oceanithermus* genus grow between pH 5.5 and 8.4 and are capable of anaerobic growth by nitrate reduction, as well as lithoheterotrophic growth with molecular hydrogen (Supplementary Material Table S3, Miroshnichenko et al., 2003). These metabolic traits align well with the bioreactor conditions.

The main archaeal and bacterial taxa identified in the collected buoyant HF and the chimney samples are illustrated in Fig. 6A, along with the mineral and chemical composition of the collected materials.

In summary, the analyzed buoyant HF and chimney samples reveal microbial diversity with various abilities of adaptations to environmental conditions, highlighting potential for selective growth in the bioreactor. Based on the metabolic functions of these taxa together with the bioreactor conditions, we can anticipate that the most abundant archaeal taxa from the chimney, Thermococci, Archaeoglobi, and Thermoprotei, are well-suited to the bioreactor conditions, likely playing active roles in sulfur and iron cycling. Among bacteria, taxa such as *Sulfurimonas*, Deinococci (mainly *Oceanithermus*), and Aquificae also from the chimney appear capable of growth by utilizing available hydrogen and sulfur compounds. Section 4.3 will examine how well these anticipated interactions unfold in the bioreactor.

4.2. Elemental and isotopic evolution of the fluid medium: impact of mineral-fluid-microorganism interactions

Based on our results, we identify four time periods during which obvious and significant chemical variations are observed in trace element concentrations (except dFe) and Sr isotopic composition of the fluid medium. These four time intervals are: 1. First fluid-inoculum interactions (0–24 h), 2. Stabilization (24–168 h), 3. Drastic change (168–264 h), and 4. Return to stabilization (264–432 h, marking the end of the experiment). Note that the changes in blood bags throughout the experiment at 0 h, 5 h, 120 h, and 288 h (see section 2.3) are unrelated to the observed chemical, mineral, or microbial diversity changes. Fig. 6B is a schematic conceptual model illustrating the mineral-fluid-microorganism interactions occurring within the gas-lift bioreactor during these four-time intervals.

4.2.1. First fluid-inoculum interactions: first 24 h

During this time interval, (i) the pH slightly increases from 6.21 to 6.66, (ii) the chemical concentrations in the fluid medium remain either constant (dNa, dK, dSi, dCl, dBr, and dBa), increase (dCa, dSO_4, and dMg), or decrease (dFe, dMn, and dLi), (iii) the $^{87}Sr/^{86}Sr$ ratio and δ^7Li value decrease, respectively, from 0.707513 to + 7.2 ‰ in the buoyant HF down to 0.707488 and + 4.6 ‰ in the fluid medium at 24 h (Table 1, Fig. 4), and (iv) Nistrosophaeria class has disappeared in the gas-lift bioreactor, with sulfur-reducing archaea classes Thermoprotei and Thermococci prevailing over the sulfate-reducing archaea of the *Archaeoglobus* genus (Fig. 5a) and no bacteria were detected suggesting there are present at very low concentration (Fig. 5b).

Between the collection time of the buoyant HF and the beginning of the gas-lift bioreactor experiment (0h), the temperature decreases from 126 °C to 80 °C, and the anhydrite saturation index shifts from being oversaturated (SI > 0) to undersaturated (SI < 0, Table 2). Consequently, anhydrite can dissolve which can explain increasing dCa and dSO_4 concentrations by up to 20 and 32%, respectively. Additionally, the increased dSO_4 concentration also change the dSr and dLi speciation to higher $SrSO_4$ and $LiSO_4^-$ concentrations (from 3.5 to 4.4% and 0.7–0.9%, respectively, Table 2). The dCa concentration increase of 4.02 mmol/L corresponds to the dissolution of 1.09 g of anhydrite, i.e., 0.8% of the inoculum. As the chimney sample was collected at immediate contact with high temperature hydrothermal fluid, we assume that the $^{87}Sr/^{86}Sr$ ratio of anhydrite is similar to that of the end-member hydrothermal fluid at the same site (0.704230 ± 0.00004, Chavagnac et al., 2018a,b; Leleu, 2017). Thus, its dissolution should induce a less radiogenic $^{87}Sr/^{86}Sr$ ratio in the fluid medium, as observed here.

Contrarily to anhydrite, pyrite and chalcopyrite as well as hematite remain oversaturated in the fluid medium (SI > 0; Table 2), allowing their potential precipitation and the drastic decrease of dFe concentrations (-67% of its initial concentration; Table 1, Fig. 4c).

Other trace metals such as dMn, and dLi also decrease in concentrations, by 24 and 22%, respectively (Fig. 4c–e). We attribute these variations to mineral precipitation, as the fluid medium is oversaturated (SI > 0) regarding to carbonate minerals, notably rhodochrosite ($MnCO_3$). The δ^7Li value decreases as well from +7.2 to +4.6 ‰ in the fluid medium. Li isotope fractionation is known to be controlled by minerals precipitation/dissolution, adsorption-desorption and ion-exchange processes (Hindshaw et al., 2019; Vigier et al., 2008; Wang et al., 2023). Thus, even if the dLi concentration and δ^7Li can be disrupt by adsorption on oxide surfaces (especially Mn-oxides, Chan and Hein, 2007), we cannot decipher here which minerals and processes can explain a lighter δ^7Li signature. Li isotopes fractionation also depends on factors such as the temperature (Millot et al., 2010; Taylor et al., 2019), the water/rock ratio (Verney-Carron et al., 2015), the pH (Li and Liu, 2020), and CO_2 concentrations in the solutions (Ji et al., 2022). However, all these factors are controlled and maintained in the bioreactor throughout the experiment.

The physico-chemical conditions in the gas-lift bioreactor (anaerobic environment maintained at 80 °C and pH ~6.5) are drastically unfavorable for the development of Nistrosophaeria, which are the most abundant archaea in the buoyant HF. They disappear from the fluid medium after 24 h of incubation (Figs. 5a and 6b). In contrast, these conditions are favorable for the preservation and growth of Archaeglobi, Thermococci, and Thermoprotei. It is noticeable that most enriched archaea that developed in the gas-lift bioreactor originated from the chimney sample (inoculum) rather than the buoyant HF, despite continuous feeding with fresh buoyant HF (Figs. 5a and 6b). With chemical features evidencing anhydrite dissolution, we anticipate that sulfate-reducing archaea such as *Archaeoglobus* would develop in such anaerobic conditions. However, *Archaeoglobus* and other Archaeoglobi are absent at 24 h which could be explained by their lowest growth rate compared to both Thermococci and Thermoprotei (Huber & Stetter, 2015a, 2015b; Zillig and Reysenbach, 2015). The occurrence of Thermoprotei and Thermococci is coherent with the physico-chemical setup of the experiment. Indeed, both classes contain (hyper)thermophilic, anaerobic, and circumneutral species capable of organotrophic growth with or without elemental sulfur. Many *Thermococcales* grow better in the presence of elemental sulfur (see section 4.1, Huber and Stetter, 2006; Le Guellec et al., 2021; Liu et al., 2012). In the gas-lift bioreactor, elemental sulfur can be provided by sulfur-bearing minerals, i.e. pyrite and chalcopyrite, present in the chimney sample (Fig. 6).

The presence of genera such as *Ferroglobus* from the Archaeoglobi class and *Thermococcus* from the Thermococci class, known for their roles in iron metabolism, could also contribute to the observed significant decrease in dFe. Indeed, *Thermococcus* reduces Fe(III), while *Ferroglobus* is capable of both oxidizing Fe(II) and reducing Fe(III) (Hafenbradl et al., 1996; Kashefi et al., 2002; Lim et al., 2020; Slobodkina et al., 2009; Tor and Lovley, 2001; Zeng et al., 2021).

4.2.2. Stabilization: 24 h–144 h

During this time interval, (i) the pH remains mainly stable around 6.6, (ii) the chemical concentrations in the fluid medium remain essentially constant, with slight reductions of dCa, dSO_4, dMn, and dSr concentrations (Fig. 4a, b, and d), (iii) the $^{87}Sr/^{86}Sr$ ratios remain stable at 0.707488 ± 0.000005, contrary to the δ^7Li value of the fluid medium, which fluctuates between +4.0 and + 7.0 ‰ (Table 1, Fig. 4d and e), (iv) Thermococci are the most abundant archaea and Thermoprotei and Archaeoglobi are present, (v) only bacteria from the genus *Sulfurimonas* and Deinococci class are significantly abundant, with *Sulfurimonas* being the most prevalent (Fig. 6b).

The observed covariations of dCa, dSO_4 and dSr concentrations

would suggest anhydrite ($CaSO_4$) precipitation. However, the fluid medium is undersaturated regarding this mineral (SI < 0), precluding its precipitation (Table 2). Instead, the concomitant decrease in dCa and dSr concentrations could be related to calcite precipitation (SI > 0, Table 2). Calcium concentrations in the fluid medium (24.39 mmol/L) are sufficiently high to support this process. In aqueous environments, where approximately 90% of total dissolved inorganic carbon is in the form of bicarbonate ions (~2 mmol/L, Dickson, 2010), calcite precipitation can occur at calcium concentrations as low as 1 mmol/L under near-neutral pH conditions (Ghobadi Nia et al., 2010). During the interval of interest, PHREEQC modeling indicates bicarbonate (HCO_3^-) concentrations ranging from 9.59 to 17.00 mmol/L, further supporting the plausibility of calcite precipitation in the experimental setup. This aligns with the oversaturation of calcite indicated by PHREEQC modeling. In another gas-lift bioreactor study, Callac et al. (2015) also observed a concomitant evolution of dCa and dSr concentrations, which was attributed to calcite - fluid medium interaction. The presence of calcite within the interstices of natural anhydrite chimney walls was previously identified by Pagé et al. (2008). Calcite precipitation induces Li isotope fractionation with a factor ranging from −8 to +2 ‰ depending on pH values and calcite growth rates (Füger et al., 2019, 2022; Marriott et al., 2004a; Marriott et al., 2004b; Seyedali et al., 2021). This fractionation may occur due to Li^+ adsorption processes onto calcite surfaces (Füger et al., 2019, 2022). The large range of fractionation factor could explain the δ^7Li variability observed in our study, between +4.0 and + 7.0 ‰. The presence of *Archaeoglobus* is also consistent with calcite precipitation, as these sulfate reducing prokaryotes contribute to the total carbon mineralization process in marine sediments as (Barton et al., 2014). Their metabolism use dSO_4 which is aligns with the observed dSO_4 decrease. Another carbonate mineral that can precipitate here is Rhodochrosite (SI > 0), whereby its precipitation could explain the observed decrease in dMn concentrations (Fig. 4C).

Data on bacterial diversity in the fluid medium are available starting 96 h after the start of the experiment (Fig. 5b). Among the bacteria identified in the buoyant HF and in the chimney sample (see section 4.1), only, *Sulfurimonas* genus from the *Campylobacterales* order and Deinococci class, are significantly abundant with *Sulfurimonas* largely dominating the diversity (Fig. 5b–Supplementary Material Table S2). As for the archaeal diversity, the most enriched bacteria thriving in the gas-lift bioreactor originates from the chimney sample rather than the buoyant HF. Mesophilic bacteria from *Sulfurimonas* genus was not expected to grow at such temperature (~80 °C) in the bioreactor (Supplementary Material Table S3). Nonetheless, *Sulfurimonas* genus was identified in various mesophilic and thermophilic hydrothermal habitats, including plumes, sediments, chimneys, and diffuse-flow fluids (Akerman et al., 2013; Hu et al., 2021; Inagaki, 2003; Li et al., 2020; Mino et al., 2017; Nakagawa et al., 2005). The presence of species at temperatures significatively above their known optimal growth temperature, such as *Sulfurimonas*, has previously been described in bioreactor enrichment culture experiments (Callac et al., 2015; Postec et al., 2005). Aquificae, mainly *Persephonella* species, originating from the chimney sample, are initially detected at extremely low abundance (<1%) in the fluid medium. However, their abundance increases to approximately 10% by 144 h, comparable to that of the chimney sample (Supplementary Material Table S2, Fig. 5b). This is consistent with the known growth conditions of *Persephonella* species, which are suitable for our culture system (François et al., 2021). Here, the gas-lift bioreactor physico-chemical conditions (gas-flux composition and pyrite and chalcopyrite in the inoculum) provides all the essential growth prerequisites for Deinococci, and Aquificae.

4.2.3. Drastic change: 168h–264h

During this time interval, drastic changes are observed regarding trace element concentrations and their isotopes. Indeed, (i) the pH slightly increasing from 6.60 to 6.97; (ii) major element concentrations remain overall constant; (iii) all trace element concentrations (apart from dFe), drastically increase by a factor of two; (iv) the $^{87}Sr/^{86}Sr$ ratio drastically decreases reaching a minimum value of 0.707337 at 264 h, while δ^7Li values continue to fluctuate between +4.0 and 7.3‰, (v) Archaeoglobi class progressively disappears; and (vi) the bacterial diversity (mainly *Sulfurimonas* and Deinococci) remains overall unchanged (Fig. 6b).

The mineral dissolution/precipitation does not explain the drastic trace elements increase. Indeed, the observed drastic increase of dMn, dLi, and dBa concentrations cannot be due to rhodochrosite and barite dissolution as the fluid medium is oversaturated regarding to both of them. The observed increase of dSr concentrations cannot be due to anhydrite dissolution even if anhydrite could dissolve (SI < 0), and supply dSr in the fluid medium. The increase of dSr concentrations by up to 74 μmol/L would imply the dissolution of 9 g of anhydrite (assuming a Sr concentration ~1500 ppm in anhydrite (Humphris and Bach, 2005), leading to a dCa and dSO_4 increase by up to 32 mmol/L, which is not observed here. Apart from dissolution-precipitation, adsorption-desorption and ion-exchange processes can also influence elemental and isotopic fluid compositions, particularly in systems with clays and reactive mineral surfaces (e.g., Huang et al., 2022; Li and Liu, 2020; Vigier et al., 2008). Li isotopes, for example, fractionate during adsorption onto clay minerals and Mn oxides, where the lighter ^{6}Li is preferentially adsorbed, leaving the fluid enriched in heavier ^{7}Li (Hindshaw et al., 2019; Li and Liu, 2020; Pistiner and Henderson, 2003; Vigier et al., 2008). Similarly, sorption-desorption effects can also influence Sr isotopes ratio (Boyer et al., 2018; Huang et al., 2022; Wallace et al., 2012). For instance, increases in $^{87}Sr/^{86}Sr$ ratios are observed in groundwater where Sr exchange on clays and mineral dissolution coexist (Johnson et al., 1997). Studies indicate that reversible Sr adsorption is also possible but varies significantly with substrate properties (Boyer et al., 2018; Gao et al., 2003). Given the observed decrease in the $^{87}Sr/^{86}Sr$ ratios, the isotopic shifts during this interval may come from Sr desorption from unradiogenic mineral or microbial surfaces. Previous studies have documented trace element sorption onto microbial surfaces (Jackson and Leppard, 2002; Violante et al., 2007), and organic and inorganic ligands are known to significantly influence cation sorption (Violante et al., 2007). With these factors in mind, the potential impact of microbial diversity on the observed trace metal and isotopes changes has to be addressed.

The bacterial diversity (mainly *Sulfurimonas* and Deinococci) and their relative abundance (66–82 % and 9–23%, respectively), remain overall constant. However, Archaeoglobi abundance seems to decrease over time, while sulfur-reducing archaea classes, i.e. Thermoprotei and Thermococci, are much more abundant, reaching both a relative abundance of 50% at 264 h. We observed that the progressive Archaeglobi class low abundance is concomitant with an increase in dSr (as well as dMn, dLi, and dBa, Fig. 4) and less radiogenic $^{87}Sr/^{86}Sr$ ratios from 0.707483 down to 0.707337 in the fluid medium. We suggest that Archaeoglobi has the potential to store many trace metals via its metabolic pathway. Indeed, to sustain their metabolic demands, bacterial and archaeal cells have to ensure the supply of the right metals to the right proteins (Waldron and Robinson, 2009). This process, known as metal homeostasis, is based on the involvement of specific genes capable of sensing, transporting and storing any metals inside and between cells (Chandrangsu et al., 2017; Waldron and Robinson, 2009). Thus, it is possible that Archaeoglobi have stored dSr in their cells with other trace metals (dMn, dLi, and dBa), and progressively release them into the fluid medium when they vanish. Such process could lead to the observed less radiogenic $^{87}Sr/^{86}Sr$ ratios from 0.707483 down to 0.707337. The δ^7Li values fluctuates between +4.0 and + 7.3 ‰ without any specific trend according to time. Poet et al. (2023) showed that membrane transporters and channels transport ^{6}Li faster than ^{7}Li. Such process associated to Archaeoglobi should result in lower δ^7Li one when they progressively disappear, which is not clearly evidenced here. Further studies on the link between Archaeoglobi class, trace metal storage and associated isotopic fractionation are therefore needed.

4.2.4. Return to stabilization: 264 h–432 h

We observed that (i) the pH remains stable at around 7 (ii) the chemical concentrations in the fluid medium either decrease (dCa, dMn, dBa, dSr, dLi), or increase (dSO_4, and dMg), (iii) the $^{87}Sr/^{86}Sr$ ratio and δ^7Li values increases reaching a maximum of 0.707794 at 432 h and +10.3 ‰ at 408 h, respectively, (iv) the abundance of archaea classes remain stable and fully dominated by sulfur-reducing ones (Thermoprotei and Thermococci, each at 50%), (iv) the abundance of the Deinococci class increases, and significant abundance of Alphaproteobacteria is observed, while the relative abundance of *Sulfurimonas* decreases (Fig. 6b).

Contrarily to the previous time intervals, the observed decrease of dCa (−13%), dSr (−26%), dMn (−55%), dLi (−51%), and dBa (−45%) concentrations is coherent with calcite, rhodochrosite and barite possible precipitation, as the fluid medium is still oversaturated regarding these minerals (SI > 0). The increase of dSO_4 (+20%) could be attributed to anhydrite dissolution (SI < 0), and no more consumption by the *Archaeoglobus* genus. However, assuming that $^{87}Sr/^{86}Sr$ ratio of anhydrite is similar to that of the end-member (see section 4.3.1), its dissolution should deliver less radiogenic $^{87}Sr/^{86}Sr$ ratio to the fluid medium which is not consistent with the drastic increase of $^{87}Sr/^{86}Sr$ ratio from 0.707337 to 0.707794 (Fig. 4D).

The microbial influence needs to be address. The relative abundance of Deinococci increases, reaching a level of abundance similar to that of *Sulfurimonas*, and is correlated with a decrease in dSr concentrations and an increase in $^{87}Sr/^{86}Sr$ ratios. We suggest that Deinococci trap dSr through either biosorption or bioaccumulation, and can potentially fractionate the Sr isotope distribution via its metabolic pathway, leading to progressive radiogenic ^{87}Sr in the fluid medium (Fig. 6b). We observe a similar behavior between Sr and Li elemental and isotopic composition (Fig. 4d and e). The δ^7Li values show a significant and progressive increase over time, i.e. from +4.6 to +10.3 ‰ (apart at 432 h). This is concomitant with dLi decrease and Deinococci class taking over the *Sulfurimonas* genus (Fig. 5b). dLi plays a role in many physiological and biochemical functions of many living organisms (Jakobsson et al., 2017). Also, dLi could be exchanged through inward flux of H+ in a regulation of intracellular toxic metal process (Swartz et al., 2005). Moreover, Poet et al. (2023) showed that Li incorporation through membrane ion channels and Na^+-Li^+/H+ exchangers fractionate Li isotopes transporting ^6Li faster than ^7Li. Such fractionation process should lead to a heavier δ^7Li signature in the fluid which is observed here. While there is currently no direct literature supporting this mechanism in Deinococci, we propose that their metabolic activity could contribute to dLi trapping, potentially decreasing dLi concentrations and enriching the fluid with a heavier δ^7Li. This hypothesis warrants further investigation to confirm its validity.

5. Conclusion

The chemical and isotopic composition of the fluid medium in the gas-lift bioreactor is influenced by mineral-fluid-microorganism interactions. The microbial diversity in the bioreactor reflects that of the sulfate-based chimney inoculum (93% anhydrite), with Archaeoglobi, Thermoprotei, Thermococci as the dominant archaea, and *Sulfurimonas* and Deinococci as the main bacteria. Over the 18-days experiment, the chemical composition of the fluid medium evolved through four distinct phases: first fluid-inoculum interactions (0–24 h), stabilization (24–168 h), drastic change (168–264 h), and return to stabilization (264–432 h). During the first fluid-inoculum interactions, sulfur-reducing archaea (Thermoprotei and Thermococci) prevailed over sulfate-reducing ones (Archaeoglobi), with fluid elemental and isotopic compositions largely controlled by mineral precipitation (sulfide minerals, rhodochrosite) and anhydrite dissolution. The stabilization phase was marked by relatively constant conditions and microbial diversity, with slight decreases in dCa, dSO_4, and dSr concentrations, consistent with calcite precipitation and Archaeoglobi sulfate-reducing metabolism. The drastic change phase featured significant increases in trace metal concentrations (dSr, dMn, dLi, and dBa) and a decrease in the $^{87}Sr/^{86}Sr$ ratio. This coincided with a decline in Archaeoglobi abundance, suggesting that these microorganisms may have released stored trace metals with a less radiogenic $^{87}Sr/^{86}Sr$ ratio into the fluid. During the return to stabilization, the elemental composition of the fluid is controlled by carbonate precipitation and anhydrite dissolution. Increases in the $^{87}Sr/^{86}Sr$ ratio and δ^7Li isotopic signature are concomitant with the increased abundance of Deinococci, suggesting possible absorption and accumulation of dSr and dLi by these bacteria.

Overall, mineral-fluid interactions primarily control major element concentrations, while trace element concentrations and isotopes are influenced by both minerals and microorganisms. Microbial processes appear to play a significant role in Sr and Li isotopic variations, but further investigation is needed to confirm these effects. These findings emphasize the need for cautious interpretation when using Sr isotopes as tracers for paleo hydrothermal records, as biological isotopic fractionation may be involved. In contrast, the fluctuations in δ^7Li signatures present challenges for its use as a reliable tracer. Further studies are needed to measure isotopic fractionation factors across minerals, fluids, and microorganisms, particularly for Sr isotopes, where microbial roles remain poorly understood. Additionally, experiments using high-pressure bioreactors could be useful to better replicate *in situ* conditions and refine our understanding of these interactions in natural hydrothermal systems.

CRediT authorship contribution statement

Lise Artigue: Writing – original draft, Visualization, Validation, Software, Project administration, Methodology, Investigation, Formal analysis, Data curation, Conceptualization. **Valérie Chavagnac:** Writing – original draft, Visualization, Validation, Supervision, Resources, Project administration, Methodology, Investigation, Funding acquisition, Formal analysis, Data curation, Conceptualization. **Christine Destrigneville:** Writing – original draft, Validation, Supervision, Software, Resources, Project administration, Methodology, Investigation, Formal analysis, Data curation, Conceptualization. **David François:** Validation, Investigation, Formal analysis, Data curation. **Françoise Lesongeur:** Investigation. **Anne Godfroy:** Writing – original draft, Validation, Supervision, Resources, Project administration, Methodology, Investigation, Funding acquisition, Formal analysis, Data curation, Conceptualization.

Data availability Statement

The original data presented in the study are included in the main article and in the Supplementary Material.

Funding

The Institut Carnot ISIFoR through the ADERA provided funding for LA, and VC. The CNRS/INSU TELLUS 2021 call provided funding for the AMINO project. The EU project Emso Eric (http://www.emso-eu.org/) provided funding for the maintenance of the EMSO-Azores observatory.

Declaration of competing interest

The authors declare that they have no known competing financial interests or personal relationships that could have appeared to influence the work reported in this paper.

Acknowledgments

We thank the *R.V. Pourquoi Pas?* and Genavir crew for their tremendous work during the MoMARsat'19. We are grateful to the chemistry facility of the Géoscience Environment Toulouse laboratory

(GET), the clean room facility of the Laboratoire d'Etudes en Geophysique et Océanographie Spatiales (LEGOS), and the mass spectrometry facility of the PANGEE platform at the Observatoire Midi-Pyrénées (OMP). We thank Céline Rommevaux for her assistance on board and her feedback on the first draft of this paper. We thank the editor and anonymous reviewers for their helpful and constructive comments.

Appendix A. Supplementary data

Supplementary data to this article can be found online at https://doi.org/10.1016/j.dsr.2025.104456.

Data availability

The original data presented in the study are included in the main article and in the Supplementary Material.

References

Akerman, N., Butterfield, D., Huber, J., 2013. Phylogenetic diversity and functional gene patterns of sulfur-oxidizing subseafloor Epsilonproteobacteria in diffuse hydrothermal vent fluids. Front. Microbiol. 4. https://www.frontiersin.org/articles/10.3389/fmicb.2013.00185.

Alain, K., Zbinden, M., Le Bris, N., Lesongeur, F., Quérellou, J., Gaill, F., Cambon-Bonavita, M., 2004. Early steps in microbial colonization processes at deep-sea hydrothermal vents. Environ. Microbiol. 6 (3), 227–241. https://doi.org/10.1111/j.1462-2920.2003.00557.x.

Andrews, M.G., Jacobson, A.D., Lehn, G.O., Horton, T.W., Craw, D., 2016. Radiogenic and stable Sr isotope ratios (87 Sr/86 Sr, δ 88/86 Sr) as tracers of riverine cation sources and biogeochemical cycling in the Milford Sound region of Fiordland, New Zealand. Geochem. Cosmochim. Acta 173, 284–303. https://doi.org/10.1016/j.gca.2015.10.005.

Araoka, D., Nishio, Y., Gamo, T., Yamaoka, K., Kawahata, H., 2016. Lithium isotopic systematics of submarine vent fluids from arc and back-arc hydrothermal systems in the western Pacific. G-cubed 17 (10), 3835–3853. https://doi.org/10.1002/2016GC006355.

Artigue, L., Chavagnac, V., Destrigneville, C., Ferron, B., Cathalot, C., 2022. Tracking the lithium and strontium isotope signature of hydrothermal plume in the water column: a Case study at the EMSO-Azores deep-sea observatory. Frontiers in Environmental Chemistry 3, 784385. https://doi.org/10.3389/fenvc.2022.784385.

Astorch-Cardona, A., Guerre, M., Dolla, A., Chavagnac, V., Rommevaux, C., 2023. Spatial comparison and temporal evolution of two marine iron-rich microbial mats from the Lucky Strike Hydrothermal Field, related to environmental variations. Front. Mar. Sci. 10, 1038192. https://doi.org/10.3389/fmars.2023.1038192.

Baker, B.J., Lesniewski, R.A., Dick, G.J., 2012. Genome-enabled transcriptomics reveals archaeal populations that drive nitrification in a deep-sea hydrothermal plume. ISME J. 6 (12), 2269–2279. https://doi.org/10.1038/ismej.2012.64.

Barker, A.K., Coogan, L.A., Gillis, K.M., Weis, D., 2008. Strontium isotope constraints on fluid flow in the sheeted dike complex of fast spreading crust: Pervasive fluid flow at Pito Deep. G-cubed 9 (6). https://doi.org/10.1029/2007GC001901 n/a-n/a.

Barton, L.L., Fardeau, M.-L., Fauque, G.D., 2014. Hydrogen sulfide: a toxic gas produced by dissimilatory sulfate and sulfur reduction and consumed by microbial oxidation. In: Kroneck, P.M.H., Torres, M.E.S. (Eds.), The Metal-Driven Biogeochemistry of Gaseous Compounds in the Environment, vol. 14. Springer, Netherlands, pp. 237–277. https://doi.org/10.1007/978-94-017-9269-1_10.

Bertoldo, C., Antranikian, G., 2006. The order Thermococcales. In: Dworkin, M., Falkow, S., Rosenberg, E., Schleifer, K.-H., Stackebrandt, E. (Eds.), The Prokaryotes: Volume 3: Archaea. Bacteria: Firmicutes, Actinomycetes. Springer, pp. 69–81. https://doi.org/10.1007/0-387-30743-5_5.

Besson, P., Degboe, J., Berge, B., Chavagnac, V., Fabre, S., Berger, G., 2014. Calcium, Na, K and Mg concentrations in seawater by inductively coupled plasma-atomic emission spectrometry: applications to IAPSO seawater reference material, hydrothermal fluids and Synthetic seawater solutions. Geostand. Geoanal. Res. 38 (3), 355–362. https://doi.org/10.1111/j.1751-908X.2013.00269.x.

Bischoff, J.L., Seyfried, W.E., 1978. Hydrothermal chemistry of seawater from 25 degrees to 350 degrees C. Am. J. Sci. 278 (6), 838–860. https://doi.org/10.2475/ajs.278.6.838.

Boeuf, D., Eppley, J.M., Mende, D.R., Malmstrom, R.R., Woyke, T., DeLong, E.F., 2021. Metapangenomics reveals depth-dependent shifts in metabolic potential for the ubiquitous marine bacterial SAR324 lineage. Microbiome 9 (1), 172. https://doi.org/10.1186/s40168-021-01119-5.

Bolyen, E., Rideout, J.R., Dillon, M.R., Bokulich, N.A., Abnet, C.C., Al-Ghalith, G.A., Alexander, H., Alm, E.J., Arumugam, M., Asnicar, F., Bai, Y., Bisanz, J.E., Bittinger, K., Brejnrod, A., Brislawn, C.J., Brown, C.T., Callahan, B.J., Caraballo-Rodríguez, A.M., Chase, J., et al., 2019. Author Correction: Reproducible, interactive, scalable and extensible microbiome data science using QIIME 2. Nat. Biotechnol. 37 (9), 1091. https://doi.org/10.1038/s41587-019-0252-6, 1091.

Boyer, A., Ning, P., Killey, D., Klukas, M., Rowan, D., Simpson, A.J., Passeport, E., 2018. Strontium adsorption and desorption in wetlands: role of organic matter functional groups and environmental implications. Water Res. 133, 27–36. https://doi.org/10.1016/j.watres.2018.01.026.

Breier, J.A., White, S.N., German, C.R., 2010. Mineral–microbe interactions in deep-sea hydrothermal systems: a challenge for Raman spectroscopy. Phil. Trans. Math. Phys. Eng. Sci. 368, 3067–3086. https://doi.org/10.1098/rsta.2010.0024, 1922.

Burger, A., Lichtscheidl, I., 2019. Strontium in the environment: Review about reactions of plants towards stable and radioactive strontium isotopes. Sci. Total Environ. 653, 1458–1512. https://doi.org/10.1016/j.scitotenv.2018.10.312.

Burggraf, S., Jannasch, H.W., Nicolaus, B., Stetter, K.O., 1990. Archaeoglobus profundus sp. nov., represents a new species within the sulfate-reducing Archaebacteria. Syst. Appl. Microbiol. 13 (1), 24–28. https://doi.org/10.1016/S0723-2020(11)80176-1.

Callac, N., Rouxel, O., Lesongeur, F., Liorzou, C., Bollinger, C., Pignet, P., Chéron, S., Fouquet, Y., Rommevaux-Jestin, C., Godfroy, A., 2015. Biogeochemical insights into microbe–mineral–fluid interactions in hydrothermal chimneys using enrichment culture. Extremophiles 19 (3), 597–617. https://doi.org/10.1007/s00792-015-0742-5.

Callahan, B.J., McMurdie, P.J., Rosen, M.J., Han, A.W., Johnson, A.J.A., Holmes, S.P., 2016. DADA2: high resolution sample inference from Illumina amplicon data. Nat. Methods 13 (7), 581–583. https://doi.org/10.1038/nmeth.3869.

Canganella, F., Gambacorta, A., Kato, C., Horikoshi, K., 2000. Effects of hydrostatic pressure and temperature on physiological traits of Thermococcus guaymasensis and Thermococcus aggregans growing on starch. Microbiol. Res. 154 (4), 297–306. https://doi.org/10.1016/S0944-5013(00)80003-8.

Cerqueira, T., Pinho, D., Froufe, H., Santos, R.S., Bettencourt, R., Egas, C., 2017. Sediment microbial diversity of three deep-sea hydrothermal vents Southwest of the Azores. Microb. Ecol. 74 (2), 332–349. https://doi.org/10.1007/s00248-017-0943-9.

Chan, L.-H., Hein, J.R., 2007. Lithium contents and isotopic compositions of ferromanganese deposits from the global ocean. Deep Sea Res. Part II Top. Stud. Oceanogr. 54 (11), 1147–1162. https://doi.org/10.1016/j.dsr2.2007.04.003.

Chandrangsu, P., Rensing, C., Helmann, J.D., 2017. Metal homeostasis and resistance in bacteria. Nat. Rev. Microbiol. 15 (6), 338–350. https://doi.org/10.1038/nrmicro.2017.15.

Charlou, J.L., Donval, J.P., Douville, E., Jean-Baptiste, P., Radford-Knoery, J., Fouquet, Y., Dapoigny, A., Stievenard, M., 2000. Compared geochemical signatures and the evolution of Menez Gwen (37°50′N) and Lucky Strike (37°17′N) hydrothermal fluids, south of the Azores Triple Junction on the Mid-Atlantic Ridge. Chem. Geol. 171 (1), 49–75. https://doi.org/10.1016/S0009-2541(00)00244-8.

Chavagnac, V., Destrigneville, C., Castillo, A., Artigue, L., 2023. Geochemistry of Hydrothermal Fluids at the Lucky Strike Hydrothermal Field Data from the EMSO-Azores Observatory. SEANOE. https://doi.org/10.17882/93190, 2021 [Data set].

Chavagnac, V., Leleu, T., Fontaine, F., Cannat, M., Ceuleneer, G., Castillo, A., 2018a. Spatial variations in vent chemistry at the Lucky Strike hydrothermal field, mid-Atlantic Ridge (37°N): Updates for subseafloor flow Geometry from the newly Discovered Capelinhos vent. G-cubed 19 (11), 4444–4458. https://doi.org/10.1029/2018GC007765.

Chavagnac, V., Saleban Ali, H., Jeandel, C., Leleu, T., Destrigneville, C., Castillo, A., Cotte, L., Waeles, M., Cathalot, C., Laes-Huon, A., Pelleter, E., Nonnotte, P., Sarradin, P.-M., Cannat, M., 2018b. Sulfate minerals control dissolved rare earth element flux and Nd isotope signature of buoyant hydrothermal plume (EMSO-Azores, 37°N Mid-Atlantic Ridge). Chem. Geol. 499, 111–125. https://doi.org/10.1016/j.chemgeo.2018.09.021.

Chowdhury, M.J., Blust, R., 2011. 7—strontium. In: Wood, C.M., Farrell, A.P., Brauner, C.J. (Eds.), Fish Physiol. 31, 351–390. https://doi.org/10.1016/S1546-5098(11)31029-1. Academic Press.

Crépeau, V., Cambon Bonavita, M.-A., Lesongeur, F., Randrianalivelo, H., Sarradin, P.-M., Sarrazin, J., Godfroy, A., 2011. Diversity and function in microbial mats from the Lucky Strike hydrothermal vent field. FEMS (Fed. Eur. Microbiol. Soc.) Microbiol. Ecol. 76 (3), 524–540. https://doi.org/10.1111/j.1574-6941.2011.01070.x.

Davis, A.C., Bickle, M.J., Teagle, D.A.H., 2003. Imbalance in the oceanic strontium budget. Earth Planet Sci. Lett. 211 (1), 173–187. https://doi.org/10.1016/S0012-821X(03)00191-2.

Dick, G.J., Anantharaman, K., Baker, B.J., Li, M., Reed, D.C., Sheik, C.S., 2013. The microbiology of deep-sea hydrothermal vent plumes: ecological and biogeographic linkages to seafloor and water column habitats. Front. Microbiol. 4. https://doi.org/10.3389/fmicb.2013.00124.

Dick, G.J., Tebo, B.M., 2010. Microbial diversity and biogeochemistry of the Guaymas Basin deep-sea hydrothermal plume. Environ. Microbiol. 12 (5), 1334–1347. https://doi.org/10.1111/j.1462-2920.2010.02177.x.

Dickson, A.G., 2010. The Carbon Dioxide System in Seawater: Equilibrium Chemistry and Measurements.

Edwards, K.J., Bach, W., McCollom, T.M., 2005. Geomicrobiology in oceanography: microbe–mineral interactions at and below the seafloor. Trends Microbiol. 13 (9), 449–456. https://doi.org/10.1016/j.tim.2005.07.005.

El Meknassi, S., Dera, G., Cardone, T., De Rafélis, M., Brahmi, C., Chavagnac, V., 2018. Sr isotope ratios of modern carbonate shells: Good and bad news for chemostratigraphy. Geology 46 (11), 1003–1006. https://doi.org/10.1130/G45380.

El Meknassi, S., Dera, G., De Rafélis, M., Brahmi, C., Lartaud, F., Hodel, F., Jeandel, C., Menjot, L., Mounic, S., Henry, M., Besson, P., Chavagnac, V., 2020. Seawater 87Sr/86Sr ratios along continental margins: patterns and processes in open and restricted shelf domains. Chem. Geol. 558, 119874. https://doi.org/10.1016/j.chemgeo.2020.119874.

Elderfield, H., Schultz, A., 1996. Mid-Ocean ridge hydrothermal fluxes and the chemical composition of the ocean. Annual Review of Earth and Planetary Science 24, 191–224. https://doi.org/10.1146/annurev.earth.24.1.191.

Erauso, G., Reysenbach, A.-L., Godfroy, A., Meunier, J.-R., Crump, B., Partensky, F., Baross, JohnA., Marteinsson, V., Barbier, G., Pace, NormanR., Prieur, D., 1993. Pyrococcus abyssi sp. Nov., a new hyperthermophilic archaeon isolated from a deep-sea hydrothermal vent. Arch. Microbiol. 160 (5). https://doi.org/10.1007/BF00252219.

Escartin, J., Barreyre, T., Cannat, M., Garcia, R., Gracias, N., Deschamps, A., Salocchi, A., Sarradin, P.-M., Ballu, V., 2015. Hydrothermal activity along the slow-spreading Lucky Strike ridge segment (Mid-Atlantic Ridge): distribution, heatflux, and geological controls. Earth Planet Sci. Lett. 431, 173–185. https://doi.org/10.1016/j.epsl.2015.09.025.

European Commission, 2020. Study on the EU's List of Critical Raw Materials. Final Report.

Flores, G.E., Campbell, J.H., Kirshtein, J.D., Meneghin, J., Podar, M., Steinberg, J.I., Seewald, J.S., Tivey, M.K., Voytek, M.A., Yang, Z.K., Reysenbach, A.-L., 2011. Microbial community structure of hydrothermal deposits from geochemically different vent fields along the Mid-Atlantic Ridge: microbial communities of hydrothermal vent deposits. Environ. Microbiol. 13 (8), 2158–2171. https://doi.org/10.1111/j.1462-2920.2011.02463.x.

Fouquet, Y., Ondréas, H., Charlou, J.-L., Donval, J.-P., Radford-Knoery, J., Costa, I., Lourenço, N.M.K.T., Tivey, M.K., 1995. Atlantic lava lakes and hot vents. Nature 377 (6546), 201. https://doi.org/10.1038/377201a0, 201.

Foustoukos, D.I., Pérez-Rodríguez, I., 2015. A continuous culture system for Assessing microbial activities in the Piezosphere. Appl. Environ. Microbiol. 81 (19), 6850–6856. https://doi.org/10.1128/AEM.01215-15.

François, D., 2021. Spatial and temporal dynamics of microbial communities in active hydrothermal vents. Université de Bretagne Occidentale tel-03609599.

François, D.X., Godfroy, A., Mathien, C., Aubé, J., Cathalot, C., Lesongeur, F., L'Haridon, S., Philippon, X., Roussel, E.G., 2021. Persephonella atlantica sp. nov.: how to adapt to physico-chemical gradients in high temperature hydrothermal habitats. Syst. Appl. Microbiol. 44 (1), 126176. https://doi.org/10.1016/j.syapm.2020.126176.

Fruchter, N., Eisenhauer, A., Dietzel, M., Fietzke, J., Böhm, F., Montagna, P., Stein, M., Lazar, B., Rodolfo-Metalpa, R., Erez, J., 2016. 88Sr/86Sr fractionation in inorganic aragonite and in corals. Geochem. Cosmochim. Acta 178, 268–280. https://doi.org/10.1016/j.gca.2016.01.039.

Füger, A., Konrad, F., Leis, A., Dietzel, M., Mavromatis, V., 2019. Effect of growth rate and pH on lithium incorporation in calcite. Geochem. Cosmochim. Acta 248, 14–24. https://doi.org/10.1016/j.gca.2018.12.040.

Füger, A., Kuessner, M., Rollion-Bard, C., Leis, A., Magna, T., Dietzel, M., Mavromatis, V., 2022. Effect of growth rate and pH on Li isotope fractionation during its incorporation in calcite. Geochem. Cosmochim. Acta 323, 276–290. https://doi.org/10.1016/j.gca.2022.02.014.

Gao, Y., Kan, A.T., Tomson, M.B., 2003. Critical Evaluation of desorption Phenomena of Heavy metals from natural sediments. Environmental Science & Technology 37 (24), 5566–5573. https://doi.org/10.1021/es034392w.

Garrity, G.M., Bell, J.A., Lilburn, T., 2005. Class I. Alphaproteobacteria class. Nov. In: Brenner, D.J., Krieg, N.R., Staley, J.T. (Eds.), Bergey's Manual® of Systematic Bacteriology: Volume Two the Proteobacteria Part C the Alpha-, Beta-, Delta-, and Epsilonproteobacteria, 1–garrity. Springer US, pp. 1–574. https://doi.org/10.1007/978-0-387-29298-4_1.

German, C.R., Casciotti, K.A., Dutay, J.-C., Heimbürger, L.E., Jenkins, W.J., Measures, C. I., Mills, R.A., Obata, H., Schlitzer, R., Tagliabue, A., Turner, D.R., Whitby, H., 2016. Hydrothermal impacts on trace element and isotope ocean biogeochemistry. Phil. Trans. Math. Phys. Eng. Sci. 374 (2081), 20160035. https://doi.org/10.1098/rsta.2016.0035.

Ghobadi Nia, M., Rahimi, H., Sohrabi, T., Naseri, A., Tofighi, H., 2010. Potential risk of calcium carbonate precipitation in agricultural drain envelopes in arid and semi-arid areas. Agric. Water Manag. 97 (10), 1602–1608. https://doi.org/10.1016/j.agwat.2010.05.014.

Godfroy, A., Postec, A., Raven, N., 2006. 4 growth of hyperthermophilic microorganisms for physiological and nutritional studies. Methods Microbiol. 35, 93–108. https://doi.org/10.1016/S0580-9517(08)70007-2. Elsevier.

Godfroy, A., Raven, N.D.H., Sharp, R.J., 2000. Physiology and continuous culture of the hyperthermophilic deep-sea vent archaeon *Pyrococcus abyssi* ST549. FEMS (Fed. Eur. Microbiol. Soc.) Microbiol. Lett. 186 (1), 127–132. https://doi.org/10.1111/j.1574-6968.2000.tb09093.x.

Gómez-Pereira, P.R., Fuchs, B.M., Alonso, C., Oliver, M.J., van Beusekom, J.E.E., Amann, R., 2010. Distinct flavobacterial communities in contrasting water masses of the North Atlantic Ocean. ISME J. 4 (4), 472–487. https://doi.org/10.1038/ismej.2009.142.

Hafenbradl, D., Keller, M., Dirmeier, R., Rachel, R., Roßnagel, P., Burggraf, S., Huber, H., Stetter, K.O., 1996. Ferroglobus placidus gen. Nov., sp. Nov., a novel hyperthermophilic archaeum that oxidizes Fe 2+ at neutral pH under anoxic conditions. Arch. Microbiol. 166 (5), 308–314. https://doi.org/10.1007/s002030050388.

Haro-Moreno, J.M., Rodriguez-Valera, F., López-García, P., Moreira, D., Martin-Cuadrado, A.-B., 2017. New insights into marine group III Euryarchaeota, from dark to light. ISME J. 11 (5), 1102–1117. https://doi.org/10.1038/ismej.2016.188.

Hartzell, P., Reed, D.W., 2006. The genus Archaeoglobus. In: Dworkin, M., Falkow, S., Rosenberg, E., Schleifer, K.-H., Stackebrandt, E. (Eds.), The Prokaryotes: Volume 3: Archaea. Bacteria: Firmicutes, Actinomycetes. Springer, pp. 82–100. https://doi.org/10.1007/0-387-30743-5_6.

Herlemann, D.P., Labrenz, M., Jürgens, K., Bertilsson, S., Waniek, J.J., Andersson, A.F., 2011. Transitions in bacterial communities along the 2000 km salinity gradient of the Baltic Sea. ISME J. 5 (10), 1571–1579. https://doi.org/10.1038/ismej.2011.41.

Hindshaw, R.S., Tosca, R., Goût, T.L., Farnan, I., Tosca, N.J., Tipper, E.T., 2019. Experimental constraints on Li isotope fractionation during clay formation. Geochem. Cosmochim. Acta 250, 219–237. https://doi.org/10.1016/j.gca.2019.02.015.

Holden, J., Breier, J., Rogers, K., Schulte, M., Toner, B., 2012. Biogeochemical processes at hydrothermal vents: Microbes and minerals, Bioenergetics, and carbon fluxes. Oceanography 25 (1), 196–208. https://doi.org/10.5670/oceanog.2012.18.

Hong, H.-J., Park, I.-S., Ryu, T., Jeong, H.S., Ryu, J., 2018. Demonstration of seawater strontium (Sr(II)) extraction and enrichment by a biosorption technique through continuous column operation. Ind. Eng. Chem. Res. 57 (38), 12909–12915. https://doi.org/10.1021/acs.iecr.8b02895.

Hu, Q., Wang, S., Lai, Q., Shao, Z., Jiang, L., 2021. Sulfurimonas indica sp. Nov., a hydrogen- and sulfur-oxidizing chemolithoautotroph isolated from a hydrothermal sulfide chimney in the Northwest Indian Ocean. Int. J. Syst. Evol. Microbiol. 71 (1). https://doi.org/10.1099/ijsem.0.004575.

Huang, T., Li, Z., Long, Y., Zhang, F., Pang, Z., 2022. Role of desorption-adsorption and ion exchange in isotopic and chemical (Li, B, and Sr) evolution of water following water–rock interaction. J. Hydrol. 610, 127800. https://doi.org/10.1016/j.jhydrol.2022.127800.

Huber, H., Jannasch, H., Rachel, R., Fuchs, T., Stetter, K.O., 1997. Archaeoglobus veneficus sp. nov., a novel facultative chemolithoautotrophic hyperthermophilic sulfite reducer, isolated from abyssal black smokers. Syst. Appl. Microbiol. 20 (3), 374–380. https://doi.org/10.1016/S0723-2020(97)80005-7.

Huber, H., Stetter, K.O., 2006. Desulfurococcales. In: Dworkin, M., Falkow, S., Rosenberg, E., Schleifer, K.-H., Stackebrandt, E. (Eds.), The Prokaryotes: Volume 3: Archaea. Bacteria: Firmicutes, Actinomycetes. Springer, pp. 52–68. https://doi.org/10.1007/0-387-30743-5_4.

Huber, H., Stetter, K.O., 2015a. Archaeoglobus. In: Bergey's Manual of Systematics of Archaea and Bacteria. John Wiley & Sons, Ltd, pp. 1–5. https://doi.org/10.1002/9781118960608.gbm00479.

Huber, H., Stetter, K.O., 2015b. Desulfurococcales ord. Nov. In: Bergey's Manual of Systematics of Archaea and Bacteria. John Wiley & Sons, Ltd, pp. 1–2. https://doi.org/10.1002/9781118960608.obm00040.

Huber, J.A., Butterfield, D.A., Baross, J.A., 2006. Diversity and distribution of subseafloor Thermococcales populations in diffuse hydrothermal vents at an active deep-sea volcano in the northeast Pacific Ocean. J. Geophys. Res.: Biogeosciences 111 (G4). https://doi.org/10.1029/2005JG000097.

Humphris, S.E., Bach, W., 2005. Strontium concentrations and isotopic compositions of anhydrites from the TAG active mound. In: Humphris, S.E., Bach, W. (Eds.), (2005): On the Sr isotope and REE compositions of anhydrites from the TAG seafloor hydrothermal syste. Geochimica et Cosmochimica Acta 69 (6), 1511–1525. *Supplement to*. https://doi.org/10.1594/PANGAEA.710795.

Inagaki, F., 2003. Sulfurimonas autotrophica gen. Nov., sp. Nov., a novel sulfur-oxidizing -proteobacterium isolated from hydrothermal sediments in the Mid-Okinawa Trough. Int. J. Syst. Evol. Microbiol. 53 (6), 1801–1805. https://doi.org/10.1099/ijs.0.02682-0.

Jackson, T.A., Leppard, G.G., 2002. Energy dispersive x-ray microanalysis and its applications in biogeochemical research. In: Violante, A., Huang, P.M., Bollag, J.-M., Gianfreda, L. (Eds.), Developments in Soil Science, vol. 28. Elsevier, pp. 219–260. https://doi.org/10.1016/S0166-2481(02)80055-1.

Jakobsson, E., Argüello-Miranda, O., Chiu, S.-W., Fazal, Z., Kruczek, J., Nunez-Corrales, S., Pandit, S., Pritchet, L., 2017. Towards a Unified understanding of lithium action in basic Biology and its significance for Applied Biology. J. Membr. Biol. 250 (6), 587–604. https://doi.org/10.1007/s00232-017-9998-2.

James, R.H., Palmer, M.R., 2000. The lithium isotope composition of international rock standards. Chem. Geol. 166 (3–4), 319–326. https://doi.org/10.1016/S0009-2541(99)00217-X.

Jeanthon, C., L'Haridon, S., Pradel, N., Prieur, D., 1999. Rapid identification of hyperthermophilic methanococci isolated from deep-sea hydrothermal vents. Int. J. Syst. Evol. Microbiol. 49 (2), 591–594. https://doi.org/10.1099/00207713-49-2-591.

Ji, T.-T., Jiang, X.-W., Gou, L.-F., Jin, Z., Zhang, H., Wan, L., Han, G., Guo, H., Wang, X.-S., 2022. Behaviors of lithium and its isotopes in groundwater with different concentrations of dissolved CO2. Geochem. Cosmochim. Acta 326, 313–327. https://doi.org/10.1016/j.gca.2022.03.038.

Johnson, J.W., Oelkers, E.H., Helgeson, H.C., 1992. SUPCRT92: a software package for calculating the standard molal thermodynamic properties of minerals, gases, aqueous species, and reactions from 1 to 5000 bar and 0 to 1000°C. Comput. Geosci. 18 (7), 899–947. https://doi.org/10.1016/0098-3004(92)90029-Q.

Johnson, K.S., Gordon, R.M., Coale, K.H., 1997. What controls dissolved iron concentrations in the world ocean? Mar. Chem. 57 (3), 137–161. https://doi.org/10.1016/S0304-4203(97)00043-1.

Jones, W.J., Leigh, J.A., Mayer, F., Woese, C.R., Wolfe, R.S., 1983. Methanococcus jannaschii sp. Nov., an extremely thermophilic methanogen from a submarine hydrothermal vent. Arch. Microbiol. 136 (4), 254–261. https://doi.org/10.1007/BF00425213.

Jones, W.J., Stugard, C.E., Jannasch, H.W., 1989. Comparison of thermophilic methanogens from submarine hydrothermal vents. Arch. Microbiol. 151 (4), 314–318. https://doi.org/10.1007/BF00406557.

Kashefi, K., Tor, J.M., Holmes, D.E., Gaw Van Praagh, C.V., Reysenbach, A.-L., Lovley, D. R., 2002. Geoglobus ahangari gen. Nov., sp. Nov., a novel hyperthermophilic archaeon capable of oxidizing organic acids and growing autotrophically on hydrogen with Fe(III) serving as the sole electron acceptor. Int. J. Syst. Evol. Microbiol. 52 (3), 719–728. https://doi.org/10.1099/ijs.0.01953-0.

Kelly, R.M., Deming, J.W., 1988. Extremely thermophilic Archaebacteria: biological and Engineering Considerations. Biotechnol. Prog. 4 (2), 47–62. https://doi.org/10.1002/btpr.5420040202.

Könneke, M., Bernhard, A.E., de la Torre, J.R., Walker, C.B., Waterbury, J.B., Stahl, D.A., 2005. Isolation of an autotrophic ammonia-oxidizing marine archaeon. Nature 437 (7058), 543–546. https://doi.org/10.1038/nature03911.

Langmuir, C., Humphris, S., Fornari, D., Van Dover, C., Von Damm, K., Tivey, M.K., Colodner, D., Charlou, J.-L., Desonie, D., Wilson, C., Fouquet, Y., Klinkhammer, G., Bougault, H., 1997. Hydrothermal vents near a mantle hot spot: the Lucky Strike vent field at 37°N on the Mid-Atlantic Ridge. Earth Planet Sci. Lett. 148 (1–2), 69–91. https://doi.org/10.1016/S0012-821X(97)00027-7.

Le Guellec, S., Leroy, E., Courtine, D., Godfroy, A., Roussel, E.G., 2021. H2-dependent formate production by hyperthermophilic Thermococcales: an alternative to sulfur reduction for reducing-equivalents disposal. ISME J. 1–14. https://doi.org/10.1038/s41396-021-01020-x.

Leleu, T., 2017. Variabilité spatio-temporelle de la composition des fluides hydrothermaux (observatoire fond de mer EMSO-Açores, Lucky Strike). Traçage de la circulation hydrothermale et quantification des flux chimiques associés. UT3 Paul Sabatier tel-01874701.

Lepage, E., Marguet, E., Geslin, C., Matte-Tailliez, O., Zillig, W., Forterre, P., Tailliez, P., 2004. Molecular diversity of new Thermococcales isolates from a Single area of hydrothermal deep-sea vents as revealed by Randomly amplified Polymorphic DNA Fingerprinting and 16S rRNA gene sequence analysis. Appl. Environ. Microbiol. 70 (3), 1277–1286. https://doi.org/10.1128/AEM.70.3.1277-1286.2004.

Li, J., Yang, J., Sun, M., Su, L., Wang, H., Gao, J., Bai, S., 2020. Distribution and Succession of microbial communities along the Dispersal pathway of hydrothermal plumes on the Southwest Indian ridge. Front. Mar. Sci. 7. https://www.frontiersin.org/articles/10.3389/fmars.2020.581381.

Li, W., Liu, X.-M., 2020. Experimental investigation of lithium isotope fractionation during kaolinite adsorption: implications for chemical weathering. Geochem. Cosmochim. Acta 284, 156–172. https://doi.org/10.1016/j.gca.2020.06.025.

Li, W., Liu, X.-M., 2022. Mineralogy and fluid chemistry controls on lithium isotope fractionation during clay adsorption. Sci. Total Environ. 851, 158138. https://doi.org/10.1016/j.scitotenv.2022.158138.

Lim, J.K., Kim, Y.J., Yang, J.-A., Namirimu, T., Yang, S.-H., Park, M.-J., Kwon, Y.M., Lee, H.S., Kang, S.G., Lee, J.-H., Kwon, K.K., 2020. Thermococcus indicus sp. nov., a Fe(III)-reducing hyperthermophilic archaeon isolated from the Onnuri vent field of the Central Indian Ocean ridge. J. Microbiol. 58 (4), 260–267. https://doi.org/10.1007/s12275-020-9424-9.

Liu, Y., Beer, L.L., Whitman, W.B., 2012. Sulfur metabolism in archaea reveals novel processes: sulfur metabolism in archaea. Environ. Microbiol. 14 (10), 2632–2644. https://doi.org/10.1111/j.1462-2920.2012.02783.x.

Marriott, C.S., Henderson, G.M., Belshaw, N.S., Tudhope, A.W., 2004a. Temperature dependence of δ7Li, δ44Ca and Li/Ca during growth of calcium carbonate. Earth Planet Sci. Lett. 222 (2), 615–624. https://doi.org/10.1016/j.epsl.2004.02.031.

Marriott, C.S., Henderson, G.M., Crompton, R., Staubwasser, M., Shaw, S., 2004b. Effect of mineralogy, salinity, and temperature on Li/Ca and Li isotope composition of calcium carbonate. Chem. Geol. 212 (1), 5–15. https://doi.org/10.1016/j.chemgeo.2004.08.002.

Marteinsson, V.T., Birrien, J.-L., Reysenbach, A.-L., Vernet, M., Marie, D., Gambacorta, A., Messner, P., Sleytr, U.B., Prieur, D., 1999a. Thermococcus barophilus sp. Nov., a new barophilic and hyperthermophilic archaeon isolated under high hydrostatic pressure from a deep-sea hydrothermal vent. Int. J. Syst. Evol. Microbiol. 49 (2), 351–359. https://doi.org/10.1099/00207713-49-2-351.

Marteinsson, V.T., Reysenbach, A.-L., Birrien, J.-L., Prieur, D., 1999b. A stress protein is induced in the deep-sea barophilic hyperthermophile Thermococcus barophilus when grown under atmospheric pressure. Extremophiles 3 (4), 277–282. https://doi.org/10.1007/s007920050128.

Martin, M., 2011. Cutadapt removes adapter sequences from high-throughput sequencing reads. EMBnet Journal 17 (1), 10–12.

McCliment, E.A., Voglesonger, K.M., O'Day, P.A., Dunn, E.E., Holloway, J.R., Cary, S.C., 2006. Colonization of nascent, deep-sea hydrothermal vents by a novel Archaeal and Nanoarchaeal assemblage. Environ. Microbiol. 8 (1), 114–125. https://doi.org/10.1111/j.1462-2920.2005.00874.x.

McNutt, R.H., 2000. Strontium isotopes. In: Cook, P.G., Herczeg, A.L. (Eds.), Environmental Tracers in Subsurface Hydrology. Springer US, pp. 233–260. https://doi.org/10.1007/978-1-4615-4557-6_8.

Mehta, N., Coutaud, M., Bouchez, J., van Zuilen, K., Bradbury, H.J., Moynier, F., Gorge, C., Skouri-Panet, F., Benzerara, K., 2023. Barium and strontium isotope fractionation by cyanobacteria forming intracellular carbonates. Geochem. Cosmochim. Acta 356, 165–178. https://doi.org/10.1016/j.gca.2023.07.014.

Miller, J.F., Almond, E.L., Shah, N.N., Ludlow, J.M., Zollweg, J.A., Streett, W.B., Zinder, S.H., Clark, D.S., 1988. High-pressure—temperature bioreactor for studying pressure—temperature relationships in bacterial growth and productivity. Biotechnol. Bioeng. 31 (5), 407–413. https://doi.org/10.1002/bit.260310503.

Millero, F.J., Feistel, R., Wright, D.G., McDougall, T.J., 2008. The composition of standard seawater and the definition of the reference-composition salinity Scale. Deep Sea Res. Oceanogr. Res. Pap. 55 (1), 50–72. https://doi.org/10.1016/j.dsr.2007.10.001.

Millot, R., Scaillet, B., Sanjuan, B., 2010. Lithium isotopes in island arc geothermal systems: Guadeloupe, Martinique (French West Indies) and experimental approach. Geochem. Cosmochim. Acta 74 (6), 1852–1871. https://doi.org/10.1016/j.gca.2009.12.007.

Mino, S., Nakagawa, S., Makita, H., Toki, T., Miyazaki, J., Sievert, S.M., Polz, M.F., Inagaki, F., Godfroy, A., Kato, S., Watanabe, H., Nunoura, T., Nakamura, K., Imachi, H., Watsuji, T., Kojima, S., Takai, K., Sawabe, T., 2017. Endemicity of the cosmopolitan mesophilic chemolithoautotroph Sulfurimonas at deep-sea hydrothermal vents. ISME J. 11 (4), 909–919. https://doi.org/10.1038/ismej.2016.178.

Miroshnichenko, M.L., L'Haridon, S., Nercessian, O., Antipov, A.N., Kostrikina, N.A., Tindall, B.J., Schumann, P., Spring, S., Stackebrandt, E., Bonch-Osmolovskaya, E.A., Jeanthon, C., 2003. Vulcanithermus mediatlanticus gen. Nov., sp. Nov., a novel member of the family Thermaceae from a deep-sea hot vent. Int. J. Syst. Evol. Microbiol. 53 (4), 1143–1148. https://doi.org/10.1099/ijs.0.02579-0.

Molari, M., Hassenrueck, C., Laso-Pérez, R., Wegener, G., Offre, P., Scilipoti, S., Boetius, A., 2023. A hydrogenotrophic Sulfurimonas is globally abundant in deep-sea oxygen-saturated hydrothermal plumes. Nature Microbiology 8 (4), 651–665. https://doi.org/10.1038/s41564-023-01342-w.

Mori, K., Maruyama, A., Urabe, T., Suzuki, K. -i., Hanada, S., 2008. Archaeoglobus infectus sp. Nov., a novel thermophilic, chemolithoheterotrophic archaeon isolated from a deep-sea rock collected at Suiyo Seamount, Izu-Bonin Arc, western Pacific Ocean. Int. J. Syst. Evol. Microbiol. 58 (4), 810–816. https://doi.org/10.1099/ijs.0.65422-0.

Morris, R.M., Rappé, M.S., Connon, S.A., Vergin, K.L., Siebold, W.A., Carlson, C.A., Giovannoni, S.J., 2002. SAR11 clade dominates ocean surface bacterioplankton communities. Nature 420 (6917), 806–810. https://doi.org/10.1038/nature01240.

Müller, M.N., Krabbenhöft, A., Vollstaedt, H., Brandini, F.P., Eisenhauer, A., 2018. Stable isotope fractionation of strontium in coccolithophore calcite: influence of temperature and carbonate chemistry. Geobiology 16 (3), 297–306. https://doi.org/10.1111/gbi.12276.

Nakagawa, S., Takai, K., Inagaki, F., Hirayama, H., Nunoura, T., Horikoshi, K., Sako, Y., 2005. Distribution, phylogenetic diversity and physiological characteristics of epsilon-Proteobacteria in a deep-sea hydrothermal field. Environ. Microbiol. 7 (10), 1619–1632. https://doi.org/10.1111/j.1462-2920.2005.00856.x.

Nelson, C.M., Schuppenhauer, M.R., Clark, D.S., 1992. High-pressure, high-temperature bioreactor for comparing effects of hyperbaric and hydrostatic pressure on bacterial growth. Appl. Environ. Microbiol. 58 (5), 1789–1793. https://doi.org/10.1128/aem.58.5.1789-1793.1992.

Neymark, L.A., Premo, W.R., Mel'nikov, N.N., Emsbo, P., 2014. Precise Determination of d88Sr in Rocks, Minerals, and Waters by Double-Spike TIMS: a Powerful Tool in the Study of Geological, Hydrological and Biological Processes. J.Anal.At.Spectrom. 29 (65). https://doi.org/10.1039/c3ja50310k.

Offre, P., Spang, A., Schleper, C., 2013. Archaea in biogeochemical cycles. Annu. Rev. Microbiol. 67 (1), 437–457. https://doi.org/10.1146/annurev-micro-092412-155614.

Olesen, S.W., Duvallet, C., Alm, E.J., 2017. dbOTU3: a new implementation of distribution-based OTU calling. PLoS One 12 (5), e0176335. https://doi.org/10.1371/journal.pone.0176335.

Ondréas, H., Cannat, M., Fouquet, Y., Normand, A., Sarradin, P.M., Sarrazin, J., 2009. Recent volcanic events and the distribution of hydrothermal venting at the Lucky Strike hydrothermal field, Mid-Atlantic Ridge. G-cubed 10 (2). https://doi.org/10.1029/2008GC002171.

Pagé, A., Tivey, M.K., Stakes, D.S., Reysenbach, A.-L., 2008. Temporal and spatial archaeal colonization of hydrothermal vent deposits. Environ. Microbiol. 10 (4), 874–884. https://doi.org/10.1111/j.1462-2920.2007.01505.x.

Parkhurst, D.L., Appelo, C.A.J., 2013. Description of input and examples for PHREEQC version 3: a computer program for speciation, batch-reaction, one-dimensional transport, and inverse geochemical calculations. USGS Numbered Series No. 6-A43; Techniques and Methods, Vols. 6-A43. U.S. Geological Survey, p. 519. https://doi.org/10.3133/tm6A43.

Pester, N.J., Reeves, E.P., Rough, M.E., Ding, K., Seewald, J.S., Seyfried, W.E., 2012. Subseafloor phase equilibria in high-temperature hydrothermal fluids of the Lucky Strike Seamount (Mid-Atlantic Ridge, 37°17′N). Geochem. Cosmochim. Acta 90, 303–322. https://doi.org/10.1016/j.gca.2012.05.018.

Pin, C., Gannoun, A., Dupont, A., 2014. Rapid, simultaneous separation of Sr, Pb, and Nd by extraction chromatography prior to isotope ratios determination by TIMS and MC-ICP-MS. Journal of Analytical Atomic Spectrometry 29. https://doi.org/10.1039/C4JA00169A.

Pistiner, J.S., Henderson, G.M., 2003. Lithium-isotope fractionation during continental weathering processes. Earth Planet Sci. Lett. 214 (1), 327–339. https://doi.org/10.1016/S0012-821X(03)00348-0.

Poet, M., Vigier, N., Bouret, Y., Jarretou, G., Gautier, R., Bendahhou, S., Balter, V., Montanes, M., Thibon, F., Counillon, L., 2023. Biological fractionation of lithium isotopes by cellular Na+/H+ exchangers unravels fundamental transport mechanisms. iScience 26 (6). https://doi.org/10.1016/j.isci.2023.106887.

Postec, A., Lesongeur, F., Pignet, P., Ollivier, B., Querellou, J., Godfroy, A., 2007. Continuous enrichment cultures: insights into prokaryotic diversity and metabolic interactions in deep-sea vent chimneys. Extremophiles 11 (6), 747–757. https://doi.org/10.1007/s00792-007-0092-z.

Postec, A., Pignet, P., Cueff-Gauchard, V., Schmitt, A., Querellou, J., Godfroy, A., 2005a. Optimisation of growth conditions for continuous culture of the hyperthermophilic archaeon Thermococcus hydrothermalis and development of sulphur-free defined and minimal media. Res. Microbiol. 156 (1), 82–87. https://doi.org/10.1016/j.resmic.2004.08.001.

Postec, A., Urios, L., Lesongeur, F., Ollivier, B., Querellou, J., Godfroy, A., 2005b. Continuous enrichment culture and molecular monitoring to investigate the microbial diversity of thermophiles inhabiting deep-sea hydrothermal ecosystems. Curr. Microbiol. 50 (3), 138–144. https://doi.org/10.1007/s00284-004-4443-z.

Qin, W., Heal, K.R., Ramdasi, R., Kobelt, J.N., Martens-Habbena, W., Bertagnolli, A.D., Amin, S.A., Walker, C.B., Urakawa, H., Könneke, M., Devol, A.H., Moffett, J.W., Armbrust, E.V., Jensen, G.J., Ingalls, A.E., Stahl, D.A., 2017. Nitrosopumilus maritimus gen. Nov., sp. Nov., Nitrosopumilus cobalaminigenes sp. Nov.,

Nitrosopumilus oxyclinae sp. Nov., and Nitrosopumilus ureiphilus sp. Nov., four marine ammonia-oxidizing archaea of the phylum Thaumarchaeota. Int. J. Syst. Evol. Microbiol. 67 (12), 5067–5079. https://doi.org/10.1099/ijsem.0.002416.

Qin, W., Martens-Habbena, W., Kobelt, J.N., Stahl, D.A., 2016. *Candidatus* Nitrosopumilus. In: Whitman, W.B., Rainey, F., Kämpfer, P., Trujillo, M., Chun, J., DeVos, P., Hedlund, B., Dedysh, S. (Eds.), Bergey's Manual of Systematics of Archaea and Bacteria, first ed. Wiley, pp. 1–9. https://doi.org/10.1002/9781118960608.gbm01290.

Quast, C., Pruesse, E., Yilmaz, P., Gerken, J., Schweer, T., Yarza, P., Peplies, J., Glöckner, F.O., 2012. The SILVA ribosomal RNA gene database project: Improved data processing and web-based tools. Nucleic Acids Res. 41 (D1), D590–D596. https://doi.org/10.1093/nar/gks1219.

Rappé, M.S., Connon, S.A., Vergin, K.L., Giovannoni, S.J., 2002. Cultivation of the ubiquitous SAR11 marine bacterioplankton clade. Nature 418 (6898), 630–633. https://doi.org/10.1038/nature00917.

Raven, N., Ladwa, N., Cossar, D., Sharp, R., 1992. Continuous culture of the hyperthermophilic archaeum Pyrococcus furiosus. Appl. Microbiol. Biotechnol. 38 (2), 263–267. https://doi.org/10.1007/BF00174480.

Reysenbach, A.-L., Huber, R., Stetter, K.O., Ishii, M., Kawasumi, T., Igarashi, Y., Eder, W., L'Haridon, S., Jeanthon, C., 2001. Phylum BI. Aquificae phy. Nov. In: Boone, D.R., Castenholz, R.W., Garrity, G.M. (Eds.), Bergey's Manual® of Systematic Bacteriology: Volume One: the Archaea and the Deeply Branching and Phototrophic Bacteria. Springer, pp. 359–367. https://doi.org/10.1007/978-0-387-21609-6_18.

Reysenbach, A.-L., Liu, Y., Banta, A.B., Beveridge, T.J., Kirshtein, J.D., Schouten, S., Tivey, M.K., Von Damm, K.L., Voytek, M.A., 2006. A ubiquitous thermoacidophilic archaeon from deep-sea hydrothermal vents. Nature 442 (7101), 444–447. https://doi.org/10.1038/nature04921.

Reysenbach, A.-L., Longnecker, K., Kirshtein, J., 2000. Novel bacterial and archaeal Lineages from an in situ growth chamber Deployed at a Mid-Atlantic Ridge hydrothermal vent. Appl. Environ. Microbiol. 66 (9), 3798–3806. https://doi.org/10.1128/AEM.66.9.3798-3806.2000.

Rinke, C., Rubino, F., Messer, L.F., Youssef, N., Parks, D.H., Chuvochina, M., Brown, M., Jeffries, T., Tyson, G.W., Seymour, J.R., Hugenholtz, P., 2019. A phylogenomic and ecological analysis of the globally abundant Marine Group II archaea (Ca. Poseidoniales ord. Nov.). ISME J. 13 (3), 663–675. https://doi.org/10.1038/s41396-018-0282-y.

Rogers, D.R., Santelli, C.M., Edwards, K.J., 2003. Geomicrobiology of deep-sea deposits: Estimating community diversity from low-temperature seafloor rocks and minerals. Geobiology 1 (2), 109–117. https://doi.org/10.1046/j.1472-4669.2003.00009.x.

Rommevaux, C., Henri, P., Degboe, J., Chavagnac, V., Lesongeur, F., Godfroy, A., Boulart, C., Destrigneville, C., Castillo, A., 2019. Prokaryote communities at active chimney and *in situ* colonization devices after a Magmatic Degassing event (37°N MAR, EMSO-Azores deep-sea observatory). G-cubed 20 (6), 3065–3089. https://doi.org/10.1029/2018GC008107.

Rosner, M., Ball, L., Peucker-Ehrenbrink, B., Blusztajn, J., Bach, W., Erzinger, J., 2007. A Simplified, accurate and fast method for lithium isotope analysis of rocks and fluids, and δ7Li values of seawater and rock reference materials. Geostand. Geoanal. Res. 31 (2), 77–88. https://doi.org/10.1111/j.1751-908X.2007.00843.x.

Ryu, J., Hong, J., Park, I.-S., Ryu, T., Hong, H.-J., 2020. Recovery of strontium (Sr2+) from seawater using a hierarchically structured MnO2/C/Fe3O4 magnetic nanocomposite. Hydrometallurgy 191, 105224. https://doi.org/10.1016/j.hydromet.2019.105224.

Santoro, A.E., Richter, R.A., Dupont, C.L., 2019. Planktonic marine archaea. Ann. Rev. Mar. Sci 11 (1), 131–158. https://doi.org/10.1146/annurev-marine-121916-063141.

Sarradin, P.-M., Legrand, J., 2019. MOMARSAT2019 cruise, RV Pourquoi pas ? https://doi.org/10.17600/18001110.

Schut, G.J., Lipscomb, G.L., Han, Y., Notey, J.S., Kelly, R.M., Adams, M.M.W., 2014. The order Thermococcales and the family Thermococcaceae. In: Rosenberg, E., DeLong, E.F., Lory, S., Stackebrandt, E., Thompson, F. (Eds.), The Prokaryotes. Springer Berlin Heidelberg, pp. 363–383. https://doi.org/10.1007/978-3-642-38954-2_324.

Seyedali, M., Coogan, L.A., Gillis, K.M., 2021. The effect of solution chemistry on elemental and isotopic fractionation of lithium during inorganic precipitation of calcite. Geochem. Cosmochim. Acta 311, 102–118. https://doi.org/10.1016/j.gca.2021.07.021.

Sheik, C.S., Jain, S., Dick, G.J., 2014. Metabolic flexibility of enigmatic SAR324 revealed through metagenomics and metatranscriptomics. Environ. Microbiol. 16 (1), 304–317. https://doi.org/10.1111/1462-2920.12165.

Sievert, S.M., Kuever, J., Muyzer, G., 2000. Identification of 16S ribosomal DNA-defined bacterial populations at a Shallow submarine hydrothermal vent near Milos island (Greece). Appl. Environ. Microbiol. 66 (7), 3102–3109.

Slobodkina, G.B., Kolganova, T.V., Querellou, J., Bonch-Osmolovskaya, E.A., Slobodkin, A.I., 2009. Geoglobus acetivorans sp. Nov., an iron(III)-reducing archaeon from a deep-sea hydrothermal vent. Int. J. Syst. Evol. Microbiol. 59 (11), 2880–2883. https://doi.org/10.1099/ijs.0.011080-0.

Stahl, D.A., 1991. Development and application of nucleic acid probes in bacterial systematics. Sequencing and Hybridization Techniques in Bacterial Systematics. https://cir.nii.ac.jp/crid/1571980075419733760.

Stevenson, E.I., Hermoso, M., Rickaby, R.E.M., Tyler, J.J., Minoletti, F., Parkinson, I.J., Mokadem, F., Burton, K.W., 2014. Controls on stable strontium isotope fractionation in coccolithophores with implications for the marine Sr cycle. Geochem. Cosmochim. Acta 128, 225–235. https://doi.org/10.1016/j.gca.2013.11.043.

Swan, B.K., Martinez-Garcia, M., Preston, C.M., Sczyrba, A., Woyke, T., Lamy, D., Reinthaler, T., Poulton, N.J., Masland, E.D.P., Gomez, M.L., Sieracki, M.E., DeLong, E.F., Herndl, G.J., Stepanauskas, R., 2011. Potential for chemolithoautotrophy among ubiquitous bacteria Lineages in the dark ocean. Science 333 (6047), 1296–1300. https://doi.org/10.1126/science.1203690.

Swartz, T.H., Ikewada, S., Ishikawa, O., Ito, M., Krulwich, T.A., 2005. The Mrp system: a giant among monovalent cation/proton antiporters? Extremophiles 9 (5), 345–354. https://doi.org/10.1007/s00792-005-0451-6.

Takai, K., Horikoshi, K., 2000. Rapid detection and Quantification of members of the archaeal community by quantitative PCR using Fluorogenic probes. Appl. Environ. Microbiol. 66 (11), 5066–5072.

Takai, K., Oida, H., Suzuki, Y., Hirayama, H., Nakagawa, S., Nunoura, T., Inagaki, F., Nealson, K.H., Horikoshi, K., 2004. Spatial distribution of marine Crenarchaeota group I in the vicinity of deep-sea hydrothermal systems. Appl. Environ. Microbiol. 70 (4), 2404–2413. https://doi.org/10.1128/AEM.70.4.2404-2413.2004.

Takai, K., Suzuki, M., Nakagawa, S., Miyazaki, M., Suzuki, Y., Inagaki, F., Horikoshi, K., 2006. Sulfurimonas paralvinellae sp. Nov., a novel mesophilic, hydrogen- and sulfur-oxidizing chemolithoautotroph within the Epsilonproteobacteria isolated from a deep-sea hydrothermal vent polychaete nest, reclassification of Thiomicrospira denitrificans as Sulfurimonas denitrificans comb. nov. and emended description of the genus Sulfurimonas. Int. J. Syst. Evol. Microbiol. 56 (8), 1725–1733. https://doi.org/10.1099/ijs.0.64255-0.

Taylor, H.L., Duivestein, I.J.K., Farkas, J., Dietzel, M., Dosseto, A., 2019. Technical note: lithium isotopes in dolostone as a palaeo-environmental proxy – an experimental approach. Clim. Past 15 (2), 635–646. https://doi.org/10.5194/cp-15-635-2019.

Teagle, D.A.H., Bickle, M.J., Alt, J.C., 2003. Recharge flux to ocean-ridge black smoker systems: a geochemical estimate from ODP Hole 504B. Earth Planet Sci. Lett. 210 (1–2), 81–89. https://doi.org/10.1016/S0012-821X(03)00126-2.

Teske, A., Hinrichs, K.-U., Edgcomb, V., de Vera Gomez, A., Kysela, D., Sylva, S.P., Sogin, M.L., Jannasch, H.W., 2002. Microbial diversity of hydrothermal sediments in the Guaymas basin: evidence for anaerobic Methanotrophic communities. Appl. Environ. Microbiol. 68 (4), 1994–2007. https://doi.org/10.1128/AEM.68.4.1994-2007.2002.

Teske, A., Wegener, G., Chanton, J.P., White, D., MacGregor, B., Hoer, D., de Beer, D., Zhuang, G., Saxton, M.A., Joye, S.B., Lizarralde, D., Soule, S.A., Ruff, S.E., 2021. Microbial communities under distinct thermal and geochemical Regimes in axial and off-Axis sediments of Guaymas basin. Front. Microbiol. 12, 633649. https://doi.org/10.3389/fmicb.2021.633649.

Thibon, F., Metian, M., Oberhänsli, F., Montanes, M., Vassileva, E., Orani, A.M., Telouk, P., Swarzenski, P., Vigier, N., 2021. Bioaccumulation of lithium isotopes in mussel Soft Tissues and implications for Coastal environments. ACS Earth Space Chem. 5 (6), 1407–1417. https://doi.org/10.1021/acsearthspacechem.1c00045.

Thibon, F., Weppe, L., Churlaud, C., Lacoue-Labarthe, T., Gasparini, S., Cherel, Y., Bustamante, P., Vigier, N., 2023. Lithium isotopes in marine food webs: effect of ecological and environmental parameters. Frontiers in Environmental Chemistry 3. https://www.frontiersin.org/articles/10.3389/fenvc.2022.1060651.

Tomascak, P.B., Magna, T., Dohmen, R., 2016. Advances in Lithium Isotope Geochemistry. Springer International Publishing. https://doi.org/10.1007/978-3-319-01430-2.

Tor, J.M., Lovley, D.R., 2001. Anaerobic degradation of aromatic compounds coupled to Fe(III) reduction by *Ferroglobus placidus*. Environ. Microbiol. 3 (4), 281–287. https://doi.org/10.1046/j.1462-2920.2001.00192.x.

Vance, D., Teagle, D.A.H., Foster, G.L., 2009. Variable Quaternary chemical weathering fluxes and imbalances in marine geochemical budgets. Nature 458 (7237), 493–496. https://doi.org/10.1038/nature07828.

Verney-Carron, A., Vigier, N., Millot, R., Hardarson, B.S., 2015. Lithium isotopes in hydrothermally altered basalts from Hengill (SW Iceland). Earth Planet Sci. Lett. 411, 62–71. https://doi.org/10.1016/j.epsl.2014.11.047.

Vigier, N., Decarreau, A., Millot, R., Carignan, J., Petit, S., France-Lanord, C., 2008. Quantifying Li isotope fractionation during smectite formation and implications for the Li cycle. Geochem. Cosmochim. Acta 72 (3), 780–792. https://doi.org/10.1016/j.gca.2007.11.011.

Vikström, H., Davidsson, S., Höök, M., 2013. Lithium availability and future production outlooks. Appl. Energy 110, 252–266. https://doi.org/10.1016/j.apenergy.2013.04.005.

Violante, A., Krishnamurti, G.S.R., Pigna, M., 2007. Factors affecting the sorption–desorption of trace elements in Soil environments. In: Violante, A., Huang, P.M., Gadd, G.M. (Eds.), Biophysico-Chemical Processes of Heavy Metals and Metalloids in Soil Environments, first ed. Wiley, pp. 169–213. https://doi.org/10.1002/9780470175484.ch5.

Von Damm, K.L., Bray, A.M., Buttermore, L.G., Oosting, S.E., 1998. The geochemical controls on vent fluids from the Lucky Strike vent field, Mid-Atlantic Ridge. Earth Planet Sci. Lett. 160 (3), 521–536. https://doi.org/10.1016/S0012-821X(98)00108-3.

Voordeckers, J.W., Do, M.H., Hügler, M., Ko, V., Sievert, S.M., Vetriani, C., 2008. Culture dependent and independent analyses of 16S rRNA and ATP citrate lyase genes: a comparison of microbial communities from different black smoker chimneys on the Mid-Atlantic Ridge. Extremophiles 12 (5), 627–640. https://doi.org/10.1007/s00792-008-0167-5.

Waite, D.W., Vanwonterghem, I., Rinke, C., Parks, D.H., Zhang, Y., Takai, K., Sievert, S.M., Simon, J., Campbell, B.J., Hanson, T.E., Woyke, T., Klotz, M.G., Hugenholtz, P., 2017. Comparative Genomic analysis of the class Epsilonproteobacteria and proposed reclassification to Epsilonbacteraeota (phyl. Nov.). Front. Microbiol. 8. https://www.frontiersin.org/articles/10.3389/fmicb.2017.00682.

Waldron, K.J., Robinson, N.J., 2009. How do bacterial cells ensure that metalloproteins get the correct metal? Nat. Rev. Microbiol. 7 (1), 25–35. https://doi.org/10.1038/nrmicro2057.

Wallace, S.H., Shaw, S., Morris, K., Small, J.S., Fuller, A.J., Burke, I.T., 2012. Effect of groundwater pH and ionic strength on strontium sorption in aquifer sediments:

implications for 90Sr mobility at contaminated nuclear sites. Appl. Geochem. 27 (8), 1482–1491. https://doi.org/10.1016/j.apgeochem.2012.04.007.
Wang, W., Jiang, S.-Y., Xiao, Y., 2023. Fluid-rock interaction effects on Li isotope behavior in continental geothermal systems. Chem. Geol. 631, 121525. https://doi.org/10.1016/j.chemgeo.2023.121525.
Wheeler, B., Cannat, M., Chavagnac, V., Fontaine, F., 2024. Diffuse venting and near seafloor hydrothermal Circulation at the Lucky Strike vent field, mid-Atlantic Ridge. G-cubed 25 (3), e2023GC011099. https://doi.org/10.1029/2023GC011099.
Whitman, W., Jeanthon, C., 2006. Methanococcales. The Prokaryotes 3, 257–273. https://doi.org/10.1007/0-387-30743-5_13.
Wissuwa, J., Bauer, S.L.M., Steen, I.H., Stokke, R., 2017. Complete genome sequence of Lutibacter profundi LP1T isolated from an Arctic deep-sea hydrothermal vent system. Standards in Genomic Sciences 12, 5. https://doi.org/10.1186/s40793-016-0219-x.
Wright, T.D., Vergin, K.L., Boyd, P.W., Giovannoni, S.J., 1997. A novel d-Subdivision Proteobacterial lineage from the lower ocean surface Layer. Appl. Environ. Microbiol. 63.
Zeng, X., Alain, K., Shao, Z., 2021. Microorganisms from deep-sea hydrothermal vents. Marine Life Science & Technology 3 (2), 204–230. https://doi.org/10.1007/s42995-020-00086-4.
Zhang, C.L., Xie, W., Martin-Cuadrado, A.-B., Rodriguez-Valera, F., 2015. Marine Group II Archaea, potentially important players in the global ocean carbon cycle. Front. Microbiol. 6. https://www.frontiersin.org/journals/microbiology/articles/10.3389/fmicb.2015.01108.
Zhang, L., Kang, M., Xu, J., Xu, J., Shuai, Y., Zhou, X., Yang, Z., Ma, K., 2016. Bacterial and archaeal communities in the deep-sea sediments of inactive hydrothermal vents in the Southwest India Ridge. Sci. Rep. 6, 25982. https://doi.org/10.1038/srep25982.
Zillig, W., Reysenbach, A.-L., 2015. Thermococci class. Nov. In: Bergey's Manual of Systematics of Archaea and Bacteria. John Wiley & Sons, Ltd, p. 1. https://doi.org/10.1002/9781118960608.cbm00030, 1.